

Article

Biosorption of Pb(II) Using Natural and Treated *Ardisia compressa* K. Leaves: Simulation Framework Extended through the Application of Artificial Neural Network and Genetic Algorithm

Alma Y. Vázquez-Sánchez ¹, Eder C. Lima ², Mohamed Abatal ^{3,*}, Rasikh Tariq ⁴, Arlette A. Santiago ⁵, Ismeli Alfonso ⁶, Claudia Aguilar ⁷ and América R. Vazquez-Olmos ⁸

- ¹ Área Agroindustrial Alimentaria, Universidad Tecnológica de Xicotepec de Juárez, Av. Universidad Tecnológica No. 1000. Col. Tierra Negra Xicotepec de Juárez, Puebla 73080, Mexico; alma.vazquez@utxicotepec.edu.mx
 - ² Institute of Chemistry, Federal University of Rio Grande do Sul (UFRGS), Av. Bento Goncalves 9500, P.O. Box 15003, Porto Alegre 91501-970, RS, Brazil; eder.lima@ufrgs.br
 - ³ Facultad de Ingeniería, Universidad Autónoma del Carmen, Campeche 24115, Mexico
 - ⁴ Institute for the Future of Education, Tecnológico de Monterrey, Monterrey 64849, Mexico; rasikhtariq@gmail.com
 - ⁵ Escuela Nacional de Estudios Superiores, Unidad Morelia, Universidad Nacional Autónoma de México, Antigua Carretera a Pátzcuaro No. 8701, Col. Ex. Hacienda de San José de la Huerta, Morelia 58190, Mexico; arlette_santiago@enesmorelia.unam.mx
 - ⁶ Instituto de Investigaciones en Materiales, Unidad Morelia, Universidad Nacional Autónoma de México, Antigua Carretera a Pátzcuaro No. 8701, Col. Ex. Hacienda de San José de la Huerta, Morelia 58190, Mexico; ialfonso@iim.unam.mx
 - ⁷ Facultad de Química, Universidad Autónoma del Carmen, Calle 56 No. 4 Av. Concordia, Ciudad del Carmen, Campeche 24180, Mexico; caguilar@pampano.unacar.mx
 - ⁸ Instituto de Ciencias aplicadas y Tecnología, UNAM, Circuito Exterior, S/N, Ciudad Universitaria, A.P. 70-186, Delegación Coyoacán, Ciudad de México 04510, Mexico; america.vazquez@icat.unam.mx
- * Correspondence: mabatal@pampano.unacar.mx; Tel.: +52-938-3811017 (ext. 1702)



Citation: Vázquez-Sánchez, A.Y.; Lima, E.C.; Abatal, M.; Tariq, R.; Santiago, A.A.; Alfonso, I.; Aguilar, C.; Vazquez-Olmos, A.R. Biosorption of Pb(II) Using Natural and Treated *Ardisia compressa* K. Leaves: Simulation Framework Extended through the Application of Artificial Neural Network and Genetic Algorithm. *Molecules* **2023**, *28*, 6387. <https://doi.org/10.3390/molecules28176387>

Academic Editors:
Monika Wawrzekiewicz and
Anna Wołowicz

Received: 12 July 2023
Revised: 15 August 2023
Accepted: 23 August 2023
Published: 31 August 2023



Copyright: © 2023 by the authors. Licensee MDPI, Basel, Switzerland. This article is an open access article distributed under the terms and conditions of the Creative Commons Attribution (CC BY) license (<https://creativecommons.org/licenses/by/4.0/>).

Abstract: This study explored the effects of solution pH, biosorbent dose, contact time, and temperature on the Pb(II) biosorption process of natural and chemically treated leaves of *A. compressa* K. (Raw-AC and AC-OH, respectively). The results show that the surface characteristics of Raw-AC changed following alkali treatment. FT-IR analysis showed the presence of various functional groups on the surface of the biosorbent, which were binding sites for the Pb(II) biosorption. The nonlinear pseudo-second-order kinetic model was found to be the best fitted to the experimental kinetic data. Adsorption equilibrium data at pH = 2–6, biosorbents dose from 5 to 20 mg/L, and temperature from 300.15 to 333.15 K were adjusted to the Langmuir, Freundlich, and Dubinin–Radushkevich (D-R) isotherm models. The results show that the adsorption capacity was enhanced with the increase in the solution pH and diminished with the increase in the temperature and biosorbent dose. It was also found that AC-OH is more effective than Raw-AC in removing Pb(II) from aqueous solutions. This was also confirmed using artificial neural networks and genetic algorithms, where it was demonstrated that the improvement was around 57.7%. The nonlinear Langmuir isotherm model was the best fitted, and the maximum adsorption capacities of Raw-AC and AC-OH were 96 mg/g and 170 mg/g, respectively. The removal efficiency of Pb(II) was maintained approximately after three adsorption and desorption cycles using 0.5 M HCl as an eluent. This research delved into the impact of solution pH, biosorbent characteristics, and operational parameters on Pb(II) biosorption, offering valuable insights for engineering education by illustrating the practical application of fundamental chemical and kinetic principles to enhance the design and optimization of sustainable water treatment systems.

Keywords: *Ardisia compressa* K.; biosorption; heavy metals; artificial neural network; educational Innovation

1. Introduction

Over recent decades, heavy metals have been monitored in sediments, soils, and water systems in different regions of the world in order to study their risks to wildlife and human health [1–3]. In these studies, the reported concentrations of various toxic metals, such as chromium (Cr), mercury (Hg), lead (Pb), nickel (Ni), and cadmium (Cd), exceed the permissible limits according to the United States Environmental Protection Agency (US-EPA) and World Health Organization (WHO) [1]. In the previous investigations, urban sewage and effluents discharged from different manufacturers like pigment, battery, and pesticides or mining activities are considered the principal sources of these hazardous metals in the monitored sites [1]. The presence of toxic metals, even at low concentrations in soils and water, can cause severe animal and human health risks, even cancer and other diseases, such as respiratory irritation, bronchial spasms, and coughing [4–6]. Therefore, intense investigations have developed various industrial and urban wastewater treatment techniques, including coagulation, chemical precipitation, reverse osmosis, ion exchange, flocculation, and membrane filtration, that are used before the waste products are discharged into the aquatic system [7]. Among these methods, adsorption has become the most used technique for removing organic or inorganic pollutants due to its simplicity, high efficiency, and low cost [8]. Numerous adsorbents have been developed for Pb(II) ion removal, such as zeolites [9], kaolinite clay [10], carbon-based materials [11], agricultural waste [12], and polymeric materials [13]. The cost and availability of the adsorbent materials are crucial to the efficiency of the adsorption technique. In this regard, many agriculture and industrial waste materials have been widely used to remove heavy metals from wastewater due to their low cost, availability, and the possibility for generation over various adsorption/desorption cycles [14–17]. A number of agro-wastes were studied for the adsorption of Pb (II) from aqueous solution, such as *Azadirachta indica* leaves [18], *Tamarindus indica* seeds [19], and rape straw [20], as a result of their chemical components namely, steroids, saponins, flavonoids, alkaloids, tannins, and amino acid [21]. Recent investigations reported that chemical modification increased the number of binding ligand groups on the biosorbent's surface. Therefore, the adsorption capacity of biosorbents is expected to be enhanced because the heavy metal ion uptake is favored by increasing active sites on the biosorbent's surface [22].

A. compressa K. belongs to the Myrsinaceae family, which is found in tropical and subtropical regions and has been used as food and folk medicine in different parts of the world [23]. In Mexico, *A. compressa* K. is found in different states, such as Aguascalientes, Chiapas, Chihuahua, Guerrero, Hidalgo, Jalisco, Michoacán, Nayarit, Oaxaca, Puebla, Tlaxcala, San Luis Potosí, Sinaloa, Tamaulipas, and Veracruz [24]. Notably, in the North of Puebla, it is known as *Acachul*, and recent investigations reported by Vázquez-Sánchez A.Y. et al. [24] and by Joaquín-Cruz, Elvia et al. [23] showed that *A. compressa* K. fruits contain various phytochemicals like anthocyanins, polyphenols, flavonoids, diterpenes, gallotannins, and chlorogenic acids. In contrast, Chandra and Mejía [25] identified the presence of phenolic constituents, such as catechin, epicatechin gallate, gallic acid, kaempferol, and ardisin, in the aqueous extracts of the leaves of *A. compressa* K. Therefore, *A. compressa* K. biomass can be considered as an alternative potential biosorbent for heavy metal removal from water due to its interesting properties and its availability.

Another novel aspect of this research is to resolve such a multivariate problem to find the optimal combination of all the tuning variables for the maximization of the removal fraction. This is attained through the application of artificial neural networks for the regression model and the genetic algorithm for optimization purposes.

To the best of our knowledge, *A. compressa* K. biomass has not been used as a biosorbent. Thus, this work contributes to studying the biosorption capacity of natural and treated-with-NaOH *A. compressa* K. leaves regarding removing Pb(II) from aqueous solutions varying solution pH, contact time, adsorbent dose, and temperature. In addition, the adsorption–desorption cycle experiments studied the reuse of raw and treated biosorbents.

2. Results and Discussion

2.1. Physicochemical Characterization

Table 1 presents the physicochemical parameters of *A. compressa* K. leaves in a sense to determine their nutritional composition. The results are in agreement with various reports of the proximate chemical composition of the other biosorbents, such as *Leucaena leucocephala* leaves [26,27] and *Nostoc commune* [28]. For example, if we compare our results with those reported for *Leucaena leucocephala* leaves, the ash content was higher than the 5.35% reported by Thamaga et al. (2021) [26] but lower than the 6.62% reported by G.W. Garcia et al. (2013) [27]; likewise, the protein contents were lower than 19.53% and 22.03% [26,27]. These variations could be attributed to differences in the ages of trees, agroclimatic conditions, and maturity stages [29]. Also, based on the results and in comparison, *N. commune* samples had a high moisture content ($96.52 \pm 0.11\%$) and high amounts of non-nitrogen-containing components ($69.56 \pm 0.09\%$) compared with *A. compressa* K. leaves. Furthermore, the values of the crude fat ($0.24 \pm 0.02\%$), crude fiber ($3.42 \pm 0.06\%$), and ash ($5.25 \pm 0.08\%$) were lower than *A. compressa* K. leaves [30].

Table 1. Physicochemical parameters of *Ardisia compressa* K. leaves.

| Parameter | Percent Composition (% w/w) |
|---------------------------|-----------------------------|
| Total soluble solids (%) | 86.49 ± 0.12 |
| Moisture (%) | 13.51 ± 0.12 |
| Ash (%) | 6.74 ± 0.01 |
| Ethereal extract (%) | 3.60 ± 0.29 |
| Raw fiber (%) | 16.51 ± 0.34 |
| Protein (%) | 5.83 ± 0.12 |
| Nitrogen-free extract (%) | 53.80 ± 0.36 |

All values are reported in % on a dry weight basis.

2.2. Characterization

2.2.1. Zero-Point Charge

Figure 1 shows the initial pH ($\text{pH}_{\text{initial}}$) variation vs. the final pH (pH_{final}) of Raw-AC and AC-OH biosorbents. As can be observed from Figure 1, the intersection of the diagonal line and the $\text{pH}_{\text{initial}}$ vs. pH_{final} curves indicates that the pH_{PZC} values of Raw-AC and AC-OH were 4.8 and 6.4, respectively. The increase in the pH_{PZC} after the alkali treatment of Raw-AC confirmed the modification in its surface charge, which might improve the biosorption of metal ions since when $\text{pH} > \text{pH}_{\text{PZC}}$, the surface becomes negative, whereas it is positive when $\text{pH} < \text{pH}_{\text{PZC}}$. Similar results were obtained and are presented in Table 2, where the pH_{PZC} values of some raw biosorbents increased with alkaline treatment.

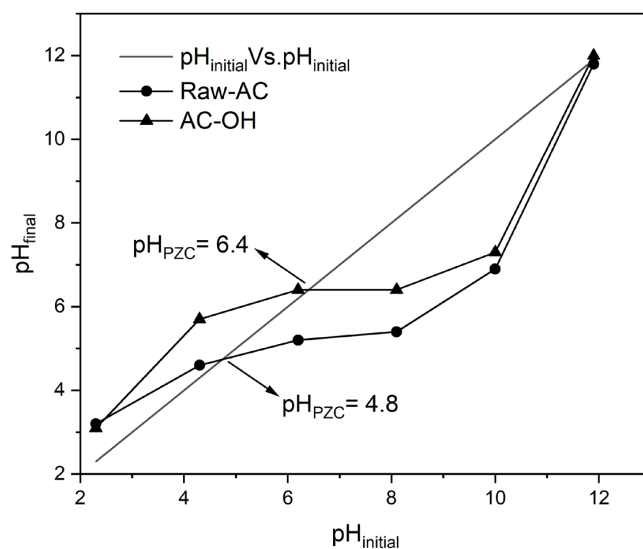


Figure 1. $\text{pH}_{\text{initial}}$ vs. pH_{final} of Raw-AC and AC-OH biosorbents.

Table 2. Comparison of pH_{PZC} values of untreated and alkaline treated biosorbents.

| Biosorbent | pH_{PZC} (Raw Biosorbent) | pH_{PZC} (Alkali-Treated Biosorbent) | Ref. |
|-----------------------------------|--|---|------------|
| <i>Prunus armeniaca</i> L. shells | 4.9 | 5.7 | [31] |
| <i>Leucaena leucephala</i> leaves | 6.7 | 7.2 | [32] |
| <i>Cupressus sempervirens</i> | 6.1 | 6.7 | [33] |
| Carob shells | 5.4 | 6.52 | [34] |
| <i>Nostoc commune</i> | 1.3 | 2.5 | [28] |
| <i>Ardisia compressa</i> K. | 4.8 | 6.4 | This study |

2.2.2. Scanning Electron Microscopy

The chemical composition before and after contact with the Pb(II) solution of the RAW-AC and AC-OH samples was estimated using energy-dispersive X-ray (EDX) spectroscopy. Both samples show mainly the presence of carbon (C), oxygen (O), calcium (Ca), and aluminum (Al). The EDX analysis results show that the amount of Pb was 4.4 Wt% for the RAW-AC sample, whereas for the AC-OH sample, the Pb adsorbed was 7.5% Wt%. These results and their corresponding SEM images of RAW-AC and AC-OH before and after contact with Pb (II) are presented in Figures 2 and 3, respectively. For both samples, the presence of Pb (II) is clear in the zoomed-in image, as represented by red dots.

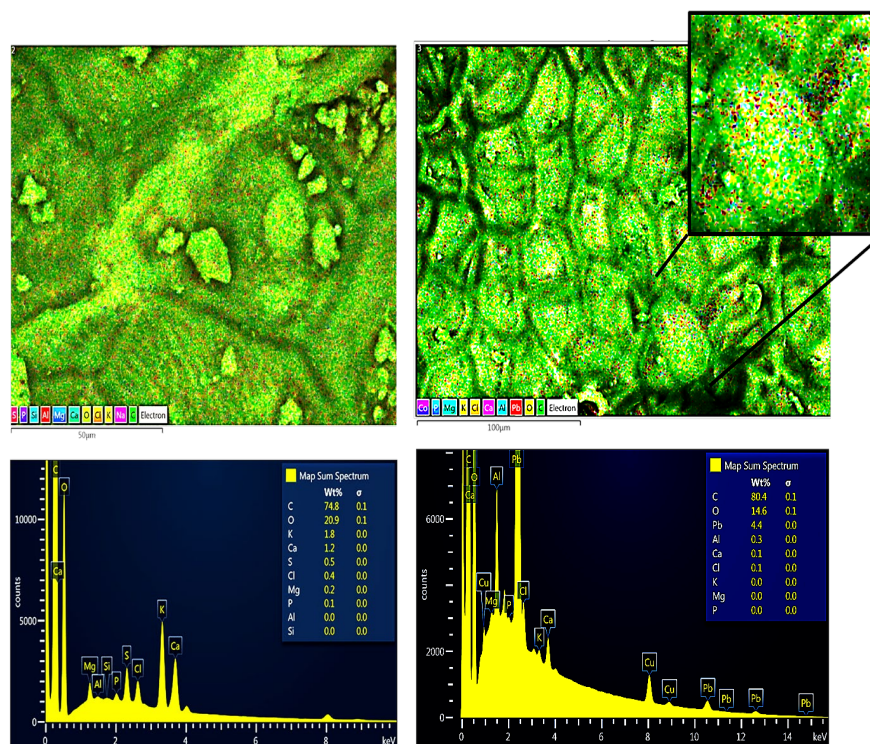


Figure 2. SEM images and EDS analysis of RAW-AC (left) and RAW-AC-Pb (right); in the zoomed-in image, the red dots represent the Pb(II) on the surface of the sample.

2.2.3. FTIR Analysis

Fourier transform infrared (FTIR) analysis of the biosorbent samples was performed to confirm the presence of functional groups. Figure 4 shows the bands corresponding to the identified functional groups in the biosorbents. The broad band, observed from 3310 to 3280 cm^{-1} for both the before-biosorption and after-biosorption samples, indicates the presence of -OH and -N-H groups [35]. The bands at 2920 , 2900 , and 2850 cm^{-1} represent the existence of methyl and methylene groups. The bands at 1730 and 1610 cm^{-1} represent the characteristics of the carbonyl group (C=O) stretching from aldehydes and ketones, which could be conjugated or non-conjugated to aromatic rings [36]. The bands at

1450 cm^{-1} show CH_2 and CH_3 groups, while the 1160 and 1220 cm^{-1} bands illustrate C-N [37]. The band at 1610 cm^{-1} was shifted to 1590 cm^{-1} after the Pb(II) uptake, suggesting the interaction of the carbonyl group with Pb(II) during the biosorption process. The *A. compressa* K. has a band at 1030 cm^{-1} and was assigned to the stretch of the C-O group of ether or ester. After the Pb(II) uptake, this band was shifted to 1020 cm^{-1} , indicating the interaction of biomass with Pb(II) [38]. As expected, the surface of the biosorbents contains different functional groups, such as carboxyl, hydroxyl, and amino groups, which could be a potential adsorption site for biosorption.

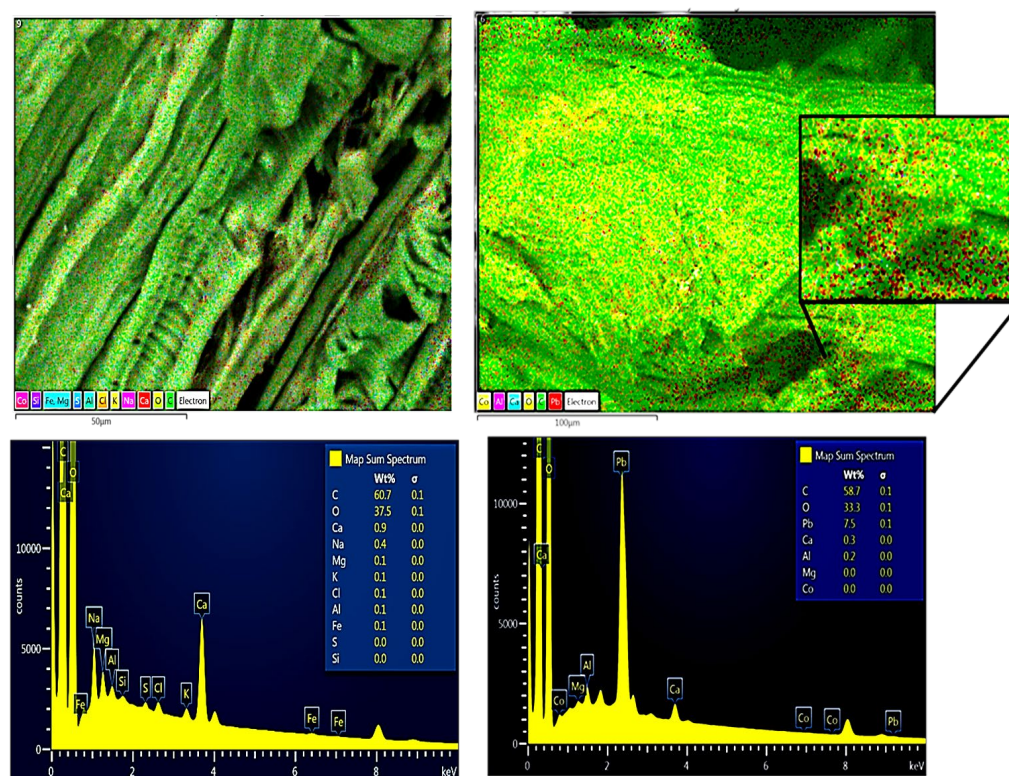


Figure 3. SEM images and EDS analysis of AC-OH (left) and AC-OH-Pb (right); in the zoomed-in image, the red dots represent the Pb(II) on the surface of the sample.

2.3. Biosorption Results

2.3.1. Effect of Solution pH

The effect of the solution pH on the Pb(II) sorption capacity of Raw-AC and AC-OH was studied using the isotherm experiments. Figure 5 shows the isotherm adsorption of Pb(II) for solution pHs at 2, 4, and 6. As observed, the Pb(II) sorption capacity of Raw-AC and AC-OH increased with the increase in adsorbate solution pH. This dependence can be associated with the metal species present at different pH solutions and the biosorbent's surface charge [39].

The lower removal of Pb(II) at acidic pH (pH = 2 and 4) can be attributed to two reasons: (a) the competition between H^+ present in the solution and Pb^{2+} ions that are the predominant species in this pH region, and (b) the electrostatic repulsion between the Pb^{2+} and the positively charged surface of Raw-AC and AC-OH biosorbents because the solution pH was lower than pH_{PZC} (Raw-AC) = 4.8 and pH_{PZC} (AC-OH) = 6.4. At pH = 6, the capacity of adsorption of biosorbents was superior when compared with pH = 2 and 4; this can be explained by the decrease in competition between protons and cations of Pb on the surface of the biosorbent due to the lower number of protons in the solutions. Furthermore, at pH = 6, the surfaces of biosorbents became negative, and the biosorption of Pb ions was favored over the ionic states of the carboxyl, hydroxyl, and amino groups [40].

Table 3 gives the parameter values of the Langmuir, Freundlich, and Dubinin–Radushkevich isotherm models using their non-linear forms (Equations (4), (5), and (6), respectively). Comparing the correlation coefficients (R^2) obtained from the nonlinearized Langmuir, Freundlich, and Dubinin–Radushkevich isotherm models, the Langmuir model was the best fitted to the experimental equilibrium data.

Table 3. Nonlinear Langmuir, Freundlich, and Dubinin–Radushkevich isotherm parameters for Pb(II) biosorption on Raw-AC and AC-OH biomass at solution pH = 2, 4, and 6.

| pH | Model | Parameters | Raw-AC | AC-OH |
|-------|----------------------------|------------------------------|---------|---------|
| 2 | Langmuir | Q_{\max} (mg/g) | 26.4 | 43.7 |
| | | $K_L \cdot 10^{-2}$ (L/mg) | 2.001 | 59.431 |
| | | R^2 | 0.981 | 0.971 |
| | Freundlich | K_F (mg/g)(L/mg) $^{1/n}$ | 3.580 | 16.226 |
| | | n | 3.200 | 5.404 |
| | | R^2 | 0.960 | 0.924 |
| | Dubinin–Radushkevich (D-R) | Q_{\max} (mg/g) | 21.948 | 41.965 |
| | | β (mol 2 /kJ 2) | 93.593 | 0.242 |
| | | E (kJ/mol) | 0.073 | 1.437 |
| R^2 | | 0.897 | 0.917 | |
| 4 | Langmuir | Q_{\max} (mg/g) | 48.1 | 69.41 |
| | | $K_L \cdot 10^{-2}$ (L/mg) | 0.882 | 56.634 |
| | | R^2 | 0.992 | 0.984 |
| | Freundlich | K_F (mg/g)(L/mg) $^{1/n}$ | 2.229 | 23.975 |
| | | n | 2.084 | 4.979 |
| | | R^2 | 0.970 | 0.913 |
| | Dubinin–Radushkevich (D-R) | Q_{\max} (mg/g) | 34.183 | 62.050 |
| | | β (mol 2 /kJ 2) | 413.006 | 0.100 |
| | | E (kJ/mol) | 0.035 | 2.236 |
| R^2 | | 0.932 | 0.867 | |
| 6 | Langmuir | Q_{\max} (mg/g) | 96.4 | 171.0 |
| | | $K_L \cdot 10^{-2}$ (L/mg) | 0.781 | 9.076 |
| | | R^2 | 0.997 | 0.990 |
| | Freundlich | K_F (mg/g)(L/mg) $^{1/n}$ | 2.654 | 22.311 |
| | | n | 1.710 | 2.043 |
| | | R^2 | 0.992 | 0.976 |
| | Dubinin–Radushkevich (D-R) | Q_{\max} (mg/g) | 55.216 | 120.205 |
| | | β (mol 2 /kJ 2) | 239.383 | 2.729 |
| | | E (kJ/mol) | 0.046 | 0.428 |
| R^2 | | 0.910 | 0.913 | |

For Raw-AC, at pH = 2, $R^2(\text{Langmuir}) = 0.981 > R^2(\text{Freundlich}) = 0.960 > R^2(\text{Dubinin–Radushkevich}) = 0.897$; at pH = 4, $R^2(\text{Langmuir}) = 0.992 > R^2(\text{Freundlich}) = 0.970 > R^2(\text{Dubinin–Radushkevich}) = 0.932$; and at pH = 6, $R^2(\text{Langmuir}) = 0.997 > R^2(\text{Freundlich}) = 0.972 > R^2(\text{Dubinin–Radushkevich}) = 0.910$.

For AC-OH, at pH = 2, $R^2(\text{Langmuir}) = 0.971 > R^2(\text{Freundlich}) = 0.924 > R^2(\text{Dubinin–Radushkevich}) = 0.917$; at pH = 4, $R^2(\text{Langmuir}) = 0.984 > R^2(\text{Freundlich}) = 0.913 > R^2(\text{Dubinin–Radushkevich}) = 0.867$; and at pH = 6, $R^2(\text{Langmuir}) = 0.990 > R^2(\text{Freundlich}) = 0.976 > R^2(\text{Dubinin–Radushkevich}) = 0.913$.

At pH = 2, 4, and 6, the maximum sorption capacities of Raw-AC determined from the Langmuir model (Q_m) were 26.4, 48.1, and 96.4 mg/g, whereas, for AC-OH, the Q_m values were 43.7, 49.6, and 170.9 mg/g, respectively. As shown in Table 3, the values of K_L for both biosorbents decreased with the increase in solution pH (from $2.001 \cdot 10^{-2}$ to $0.781 \cdot 10^{-2}$ L/mg for Raw-AC and from $59.431 \cdot 10^{-2}$ to $9.076 \cdot 10^{-2}$ L/mg for AC-OH), indicating that

the adsorption of Pb(II) was not favored in an acidic solution. Similar results were reported using other biosorbents [39,40].

The values of the average relative error (ARE), the sum of square error (SSE), normalized standard deviation Δq (%), chi-squared test (χ^2), the sum of absolute error (EABS), and the root mean square error (RMSE) are presented in Table 4.

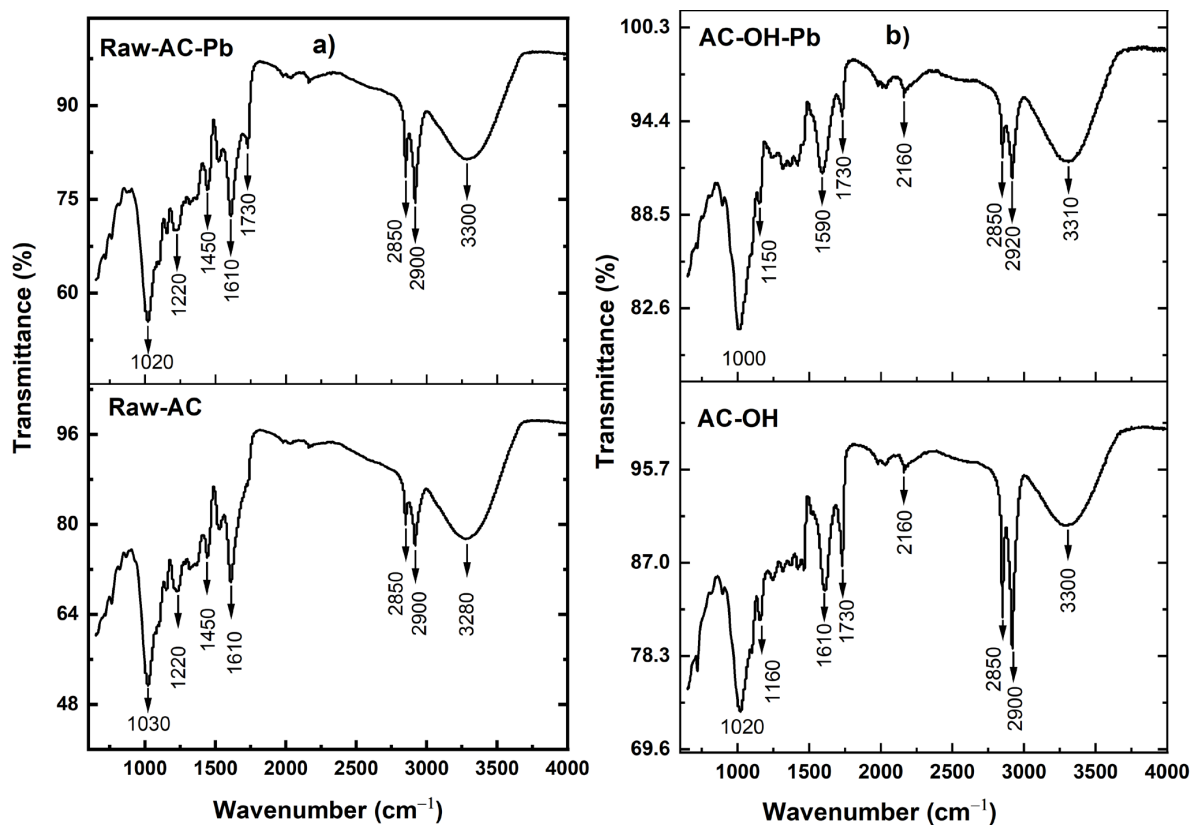


Figure 4. FTIR spectra of (a) Raw-AC and Raw-AC-Pb and (b) AC-OH and AC-OH-Pb.

Table 4. Error function values of the Langmuir, Freundlich, and Dubinin–Radushkevich isotherm models at solution pH = 2, 4, and 6.

| Biosorbent | pH | Model | Error Functions | | | | | |
|------------|----|------------|-----------------|----------|----------------|----------|--------|--------|
| | | | APE | SSE | Δq (%) | χ^2 | EABS | RMSE |
| Raw-AC | 2 | Langmuir | 9.934 | 4.703 | 19.201 | 1.790 | 5.898 | 0.970 |
| | | Freundlich | 16.261 | 21.035 | 19.881 | 1.581 | 10.604 | 2.051 |
| | | D-R | 36.483 | 51.896 | 57.739 | 353.992 | 15.899 | 3.222 |
| | 4 | Langmuir | 12.051 | 8.054 | 17.513 | 1.223 | 5.875 | 1.269 |
| | | Freundlich | 19.734 | 36.164 | 23.840 | 2.180 | 13.922 | 2.689 |
| | | D-R | 47.706 | 81.307 | 70.448 | 509.599 | 21.196 | 4.033 |
| | 6 | Langmuir | 16.786 | 9.119 | 30.325 | 3.133 | 6.721 | 1.510 |
| | | Freundlich | 17.545 | 25.427 | 29.171 | 1.516 | 12.695 | 2.255 |
| | | D-R | 53.582 | 272.070 | 72.248 | 903.793 | 41.273 | 7.377 |
| AC-OH | 2 | Langmuir | 6.402 | 54.695 | 8.453 | 3.009 | 14.617 | 3.307 |
| | | Freundlich | 17.359 | 142.978 | 24.869 | 7.253 | 28.274 | 5.347 |
| | | D-R | 30.443 | 156.436 | 47.782 | 911.672 | 30.073 | 5.593 |
| | 4 | Langmuir | 24.359 | 87.296 | 30.821 | 10.184 | 19.823 | 4.178 |
| | | Freundlich | 68.640 | 469.134 | 43.902 | 16.675 | 52.871 | 9.686 |
| | | D-R | 38.773 | 719.036 | 53.671 | 51.392 | 54.909 | 11.992 |
| | 6 | Langmuir | 16.701 | 169.569 | 21.784 | 4.109 | 25.363 | 5.824 |
| | | Freundlich | 81.765 | 402.405 | 131.184 | 16.084 | 48.817 | 8.971 |
| | | D-R | 55.164 | 1427.996 | 71.002 | 427.180 | 88.157 | 16.900 |

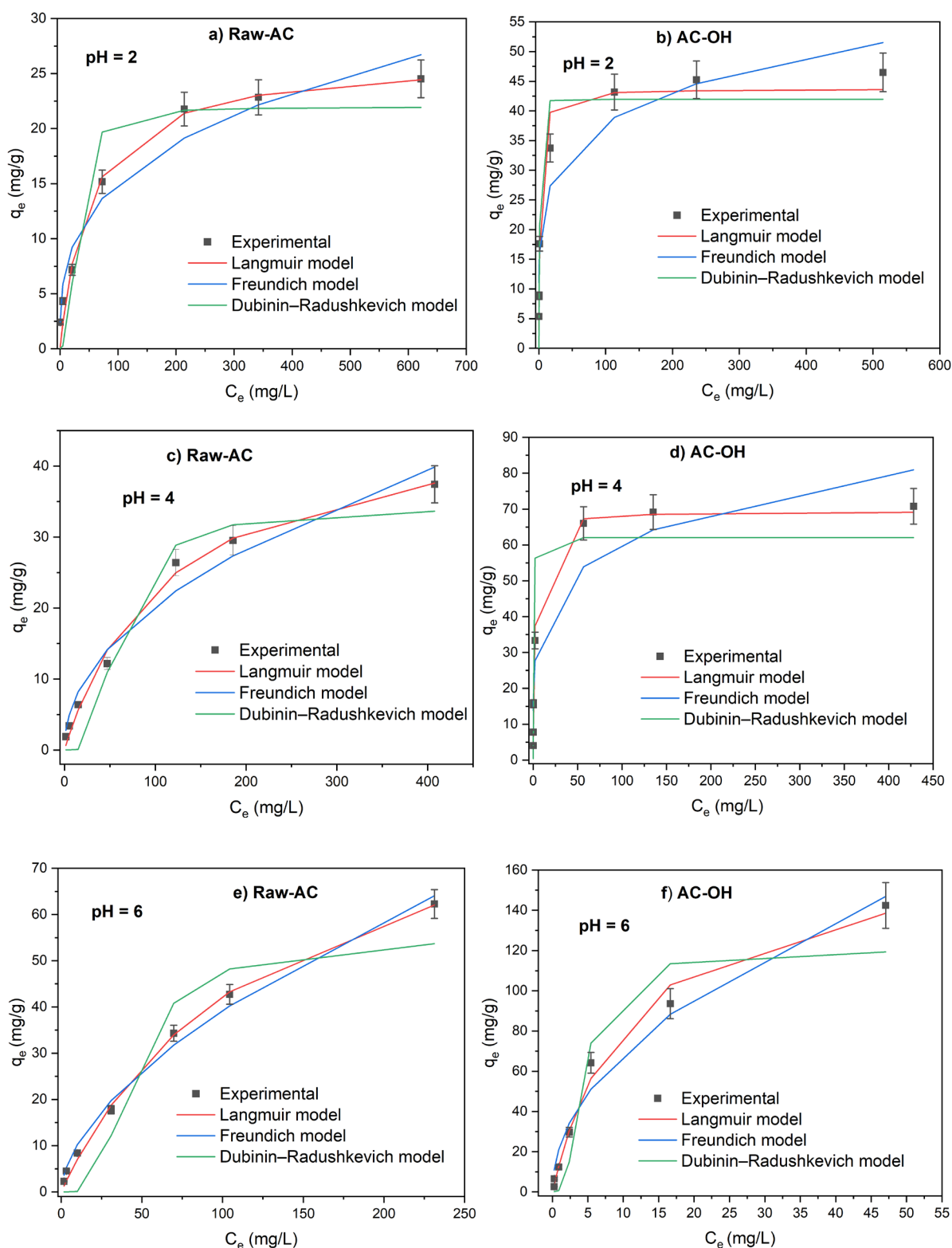


Figure 5. Adsorption isotherms of Pb(II) on Raw-AC and AC-OH at pH = 2 (a,b), pH = 4 (c,d), and pH = 6 (e,f).

Comparing the values calculated for both isotherm models, it can be observed that the lower values of all error functions were obtained for the nonlinearized Langmuir model, confirming the same result predicted using correlation coefficient nonlinear analysis.

2.3.2. Adsorbent Mass Effect

The effect of biosorbent mass on the adsorption of Pb(II) was explored using isotherm experiments. Figure 6 shows that the Pb(II) adsorption isotherms for doses of Raw-AC and AC-OH that varied from 5 to 20 g/L. The experimental data graphs were plotted alongside nonlinear Langmuir and Freundlich isotherm models.

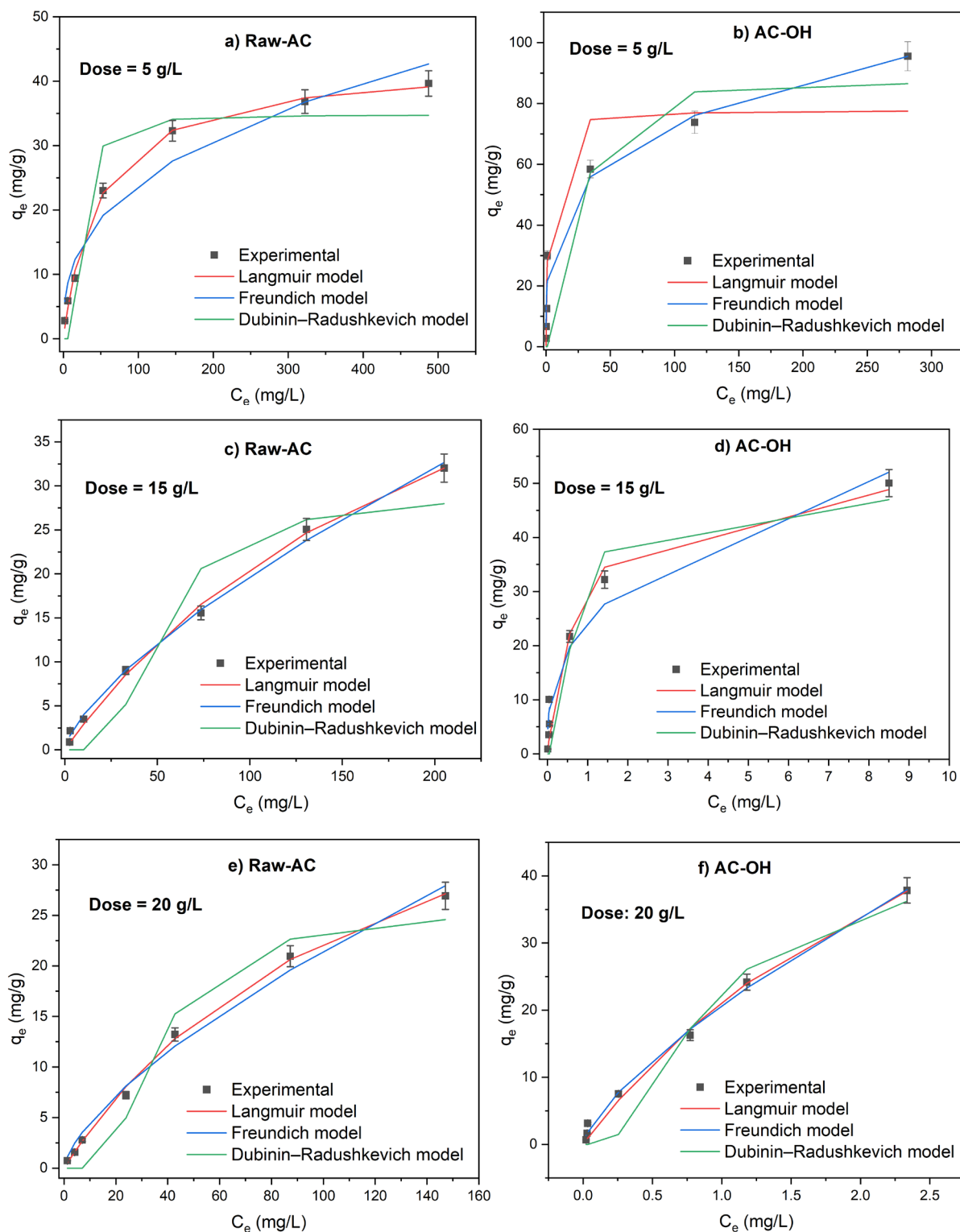


Figure 6. Adsorption isotherms of Pb(II) on Raw-AC and AC-OH at doses of 5 g/L (a,b), 15 g/L (c,d), and 20 g/L (e,f).

The removal percentage of Pb(II) was found to increase by increasing the biosorbent dose and decrease with increasing of initial concentration of Pb(II). For example, at C_i Pb(II) = 500 mg/L, the removal percentages of Pb(II) by Raw-AC and AC-OH were found to be 52.59–89.47%, 76.04–99.83%, and 86.07–99.76% at a doses of 5, 15, and 20 g/L, respectively. This result can be explained by the increase in the number of adsorption sites with increasing biosorbent mass [31].

Experimental equilibrium adsorption data were accessed using the nonlinear forms of Langmuir, Freundlich, and Dubinin–Radushkevich isotherm models. Table 5 shows the parameters of the isotherm models and their respective correlation coefficients (R^2).

Table 5. Nonlinear Langmuir, Freundlich, and Dubinin–Radushkevich isotherm parameters for Pb(II) biosorption on Raw-AC and AC-OH biomass at dose = 5 g/L, 15 g/L, and 20 g/L.

| Dose (g/L) | Model | Parameters | Raw-AC | AC-OH |
|------------|----------------------------|------------------------------|---------|---------|
| 5 | Langmuir | Q_{\max} (mg/g) | 53.7 | 73.7 |
| | | $K_L \cdot 10^{-2}$ (L/mg) | 2.105 | 0.773 |
| | | R^2 | 0.996 | 0.957 |
| | Freundlich | K_F (mg/g)(L/mg) $^{1/n}$ | 4.905 | 23.916 |
| | | n | 2.494 | 4.414 |
| | | R^2 | 0.953 | 0.953 |
| | Dubinin–Radushkevich (D-R) | Q_{\max} (mg/g) | 34.771 | 87.074 |
| | | β (mol 2 /kJ 2) | 68.942 | 81.735 |
| | | E (kJ/mol) | 0.085 | 0.078 |
| R^2 | | 0.908 | 0.836 | |
| 15 | Langmuir | Q_{\max} (mg/g) | 53.5 | 53.3 |
| | | $K_L \cdot 10^{-2}$ (L/mg) | 0.613 | 128.915 |
| | | R^2 | 0.996 | 0.966 |
| | Freundlich | K_F (mg/g)(L/mg) $^{1/n}$ | 0.952 | 24.446 |
| | | n | 1.539 | 2.829 |
| | | R^2 | 0.986 | 0.964 |
| | Dubinin–Radushkevich (D-R) | Q_{\max} (mg/g) | 29.303 | 47.476 |
| | | β (mol 2 /kJ 2) | 310.592 | 0.136 |
| | | E (kJ/mol) | 0.040 | 1.916 |
| R^2 | | 0.914 | 0.905 | |
| 20 | Langmuir | Q_{\max} (mg/g) | 50.1 | 90.6 |
| | | $K_L \cdot 10^{-2}$ (L/mg) | 0.801 | 30.554 |
| | | R^2 | 0.998 | 0.993 |
| | Freundlich | K_F (mg/g)(L/mg) $^{1/n}$ | 0.941 | 20.674 |
| | | n | 1.472 | 1.395 |
| | | R^2 | 0.989 | 0.997 |
| | Dubinin–Radushkevich (D-R) | Q_{\max} (mg/g) | 25.706 | 42.859 |
| | | β (mol 2 /kJ 2) | 157.144 | 0.212 |
| | | E (kJ/mol) | 0.056 | 1.537 |
| R^2 | | 0.955 | 0.951 | |

Based on the correlation coefficient shown, for all Raw-AC dose values, the nonlinear Langmuir isotherm model showed a better fit to the adsorption data than the Freundlich and Dubinin–Radushkevich isotherm models. The maximum adsorption capacities (q_{\max}) were 53.7 mg/g, 53.5 mg/g, and 50.1 mg/g for 5 g/L, 15 g/L, and 20 g/L of Raw-AC, respectively. The decrease in the adsorption amount with increasing biosorbent concentration has been reported in various investigations, which can be attributed to the declining total biosorbent surface area caused by the aggregation of sorption sites [41].

At biosorbent concentrations of 5 g/L and 15 g/L, experimental adsorption isotherms of AC-OH were better fitted to the Langmuir and Dubinin–Radushkevich models, whereas

at a higher biosorbent concentration (20 g/L), the biosorption data were better fitted using the Freundlich and Dubinin–Radushkevich models.

2.3.3. Effect of Contact Time

Figure 7a,b show the uptake of Pb(II) versus contact time with Raw-AC and AC-OH, respectively. It was observed that for all initial Pb(II) concentrations ranging from 25 mg/L to 250 mg/L, between 80 and 85% of Pb(II) was removed in the first 10 min of contact time. Following this time, the Pb(II) removal rate became negligible, and equilibrium was achieved in 30 min for the biosorption of Pb(II) by both biosorbents. The rapid uptake of lead ions in the first stage, which is commonly observed for biosorption of metal ions, is due to physicochemical interactions between the metal solution and available functional groups on the biomass surface [42]. As can be seen from Figure 7a,b, the equilibrium time of the biosorption process was 30 min, and after this time, the insignificant removal rate of Pb(II) could be attributed to the saturation of the available sites on the Raw-AC and AC-OH biosorbents surfaces [43].

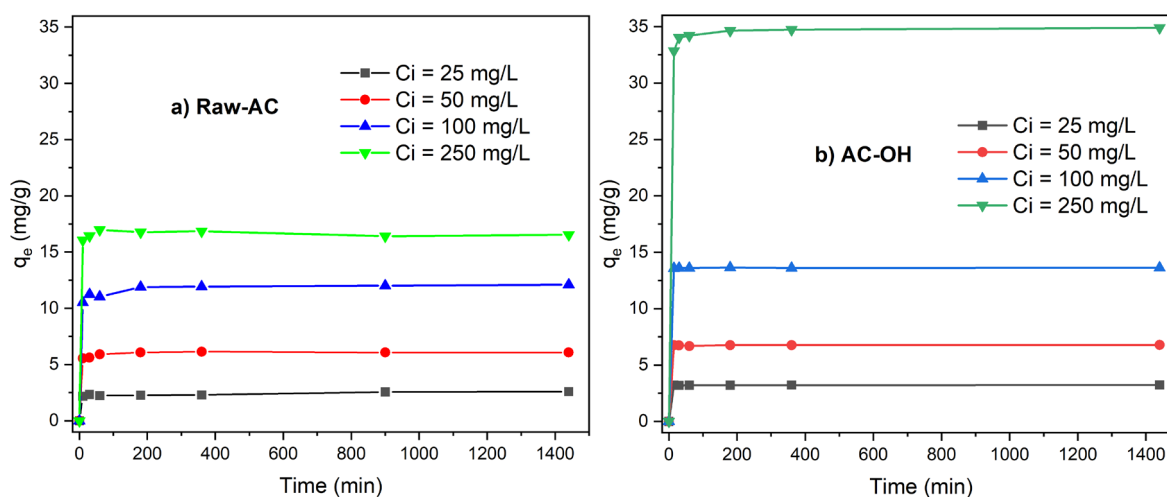


Figure 7. q_e (mg/g) vs. contact time t (min) of (a) Raw-AC and (b) AC-OH.

Table 6 shows the values of kinetic parameters of Pb(II) biosorption on Raw-AC and AC-OH biosorbents obtained from the nonlinear pseudo-first- (PFO) and pseudo-second-order (PSO) models (non-linear equations of PFO and PSO are shown in Supplementary Material).

Table 6. Parameter values calculated using the nonlinear forms of the pseudo-first-order and pseudo-second-order kinetic models for Pb(II) biosorption on Raw-AC and AC-OH biomass at $C_i = 25$ mg/L, 50 mg/L, 100 mg/L, and 250 mg/L.

| Biosorbent | C_i (mg/L) | Pseudo-First-Order | | | Pseudo-Second-Order | | |
|------------|-----------------|-----------------------|------------------|-------|-----------------------|---------------------|-------|
| | | $q_{e,cal}$ (mg/g) | k_1 (1/min) | R^2 | $q_{e,cal}$ (mg/g) | k_2 (g/mg min) | R^2 |
| Raw-AC | 25 | 2.4 | 0.341 | 0.976 | 2.4 | 0.970 | 0.994 |
| | 50 | 6.0 | 0.118 | 0.985 | 6.2 | 0.038 | 0.987 |
| | 100 | 11.7 | 0.228 | 0.941 | 11.9 | 0.058 | 0.973 |
| | 250 | 16.7 | 0.332 | 0.990 | 16.7 | 0.148 | 0.991 |
| AC-OH | 25 | 3.2 | 0.409 | 0.999 | 3.2 | 3.175 | 0.999 |
| | 50 | 6.7 | 0.298 | 0.999 | 6.8 | 0.728 | 0.999 |
| | 100 | 13.6 | 0.232 | 0.999 | 13.7 | 0.153 | 0.999 |
| | 250 | 34.5 | 0.200 | 0.997 | 34.8 | 0.032 | 1.000 |

Comparing the values of the determination coefficient (R^2) and the $q_{e,calc}$ obtained from both kinetic models, it can be observed that for all initial concentrations ($C_i(\text{Pb(II)}) = 25\text{--}250 \text{ mg/L}$), the nonlinear PSO model fit better than the PFO model. Furthermore, the PSO rate constants (k_2) were found to decrease from 0.084–0.484 to 0.024–0.148 (g mg min) for Raw-AC and from 0.488–3.175 to 0.022–0.032 (g/mg min) for AC-OH, for an increase in the concentration of Pb(II) from 25 to 250 mg/L. Biomass treated with NaOH showed a higher uptake of Pb(II) and biosorption rate k_2 compared with the raw biomass. The enhancement of biosorption capacity of treated *Ardisia compressa* K. leaves was also observed in other biosorbents [32,44].

As shown in Table 6, the regression coefficients obtained from the nonlinear form of the PSO and PSO models were higher than 0.941; furthermore, the $q_{e,cal}$ obtained by both kinetic models were similar to $q_{e,exp}$. Therefore, the comparison of R^2 and $q_{e,cal}$ resulted in inadequate criteria for defining the best-fitting kinetic model. However, the values calculated by the six function errors for all initial concentrations of Pb(II) resulted in lower PSO than the PFO (Table 7), confirming that the PSO was the best model to fit the kinetic data. This result suggests that the removal of Pb(II) was controlled by chemisorption, which involved the strong surface complexation of metal ions with the functional groups on the surface of biosorbents [31].

Table 7. Error functions of the PFO and PSO kinetic models.

| Biosorbent | Ci (mg/L) | Model | Error Functions | | | | | |
|------------|-----------|-------|-----------------|-------------------|------------------------------|------------------------|-------|-------|
| | | | ARE | SSE (10^{-2}) | $\Delta q(\%)$ (10^{-2}) | χ^2 (10^{-2}) | EABS | RMSE |
| Raw-AC | 25 | PFO | 1.486 | 1.531 | 2.099 | 0.635 | 0.251 | 0.055 |
| | | PSO | 1.285 | 1.065 | 1.728 | 0.444 | 0.218 | 0.046 |
| | 50 | PFO | 1.758 | 9.475 | 2.218 | 1.633 | 0.698 | 0.138 |
| | | PSO | 1.725 | 8.188 | 2.166 | 1.510 | 0.663 | 0.128 |
| | 100 | PFO | 2.790 | 99.482 | 3.577 | 8.505 | 2.252 | 0.446 |
| | | PSO | 1.712 | 44.854 | 2.446 | 3.874 | 1.360 | 0.300 |
| | 250 | PFO | 1.051 | 28.115 | 1.297 | 1.688 | 1.226 | 0.237 |
| | | PSO | 0.933 | 26.359 | 1.253 | 1.583 | 1.089 | 0.230 |
| AC-OH | 25 | PFO | 0.310 | 0.093 | 0.424 | 0.029 | 0.060 | 0.015 |
| | | PSO | 0.298 | 0.064 | 0.352 | 0.019 | 0.057 | 0.013 |
| | 50 | PFO | 0.318 | 0.552 | 0.495 | 0.082 | 0.128 | 0.037 |
| | | PSO | 0.295 | 0.459 | 0.452 | 0.068 | 0.119 | 0.034 |
| | 100 | PFO | 0.136 | 0.446 | 0.220 | 0.033 | 0.111 | 0.033 |
| | | PSO | 0.341 | 1.560 | 0.414 | 0.116 | 0.276 | 0.062 |
| | 250 | PFO | 0.711 | 46.737 | 0.889 | 1.355 | 1.467 | 0.342 |
| | | PSO | 0.263 | 6.943 | 0.345 | 0.204 | 0.539 | 0.132 |

2.3.4. Temperature Effect on Sorption Capacity

The study of the temperature effect on the sorption of Pb(II) was evaluated using adsorption isotherm experiments by varying the temperature from 300.15 to 330.15 K. Figure 8 shows the adsorption isotherms for Raw-AC and AC-OH at $T = 300.15, 315.15,$ and 330.15 K . It can be observed that the adsorption capacity of Pb(II) of Raw-AC and AC-OH was higher at room temperature compared with that at 315.15 and 330.15 K, confirming that the adsorption was an exothermic process. The decrease in adsorption capacity with temperature can be explained by the breaking of adsorption forces between the metal ions and active sites on the biosorbents caused by the excess of energy supplied to the system, which promoted the desorption of metal ions from surface biosorbent [45,46]. The exothermic adsorption of Pb(II) ions using various types of sor-

bents, such as *Azadirachta indica* [47], montmorillonite [45], rice husk [48], and activated tea waste [49], was previously reported.

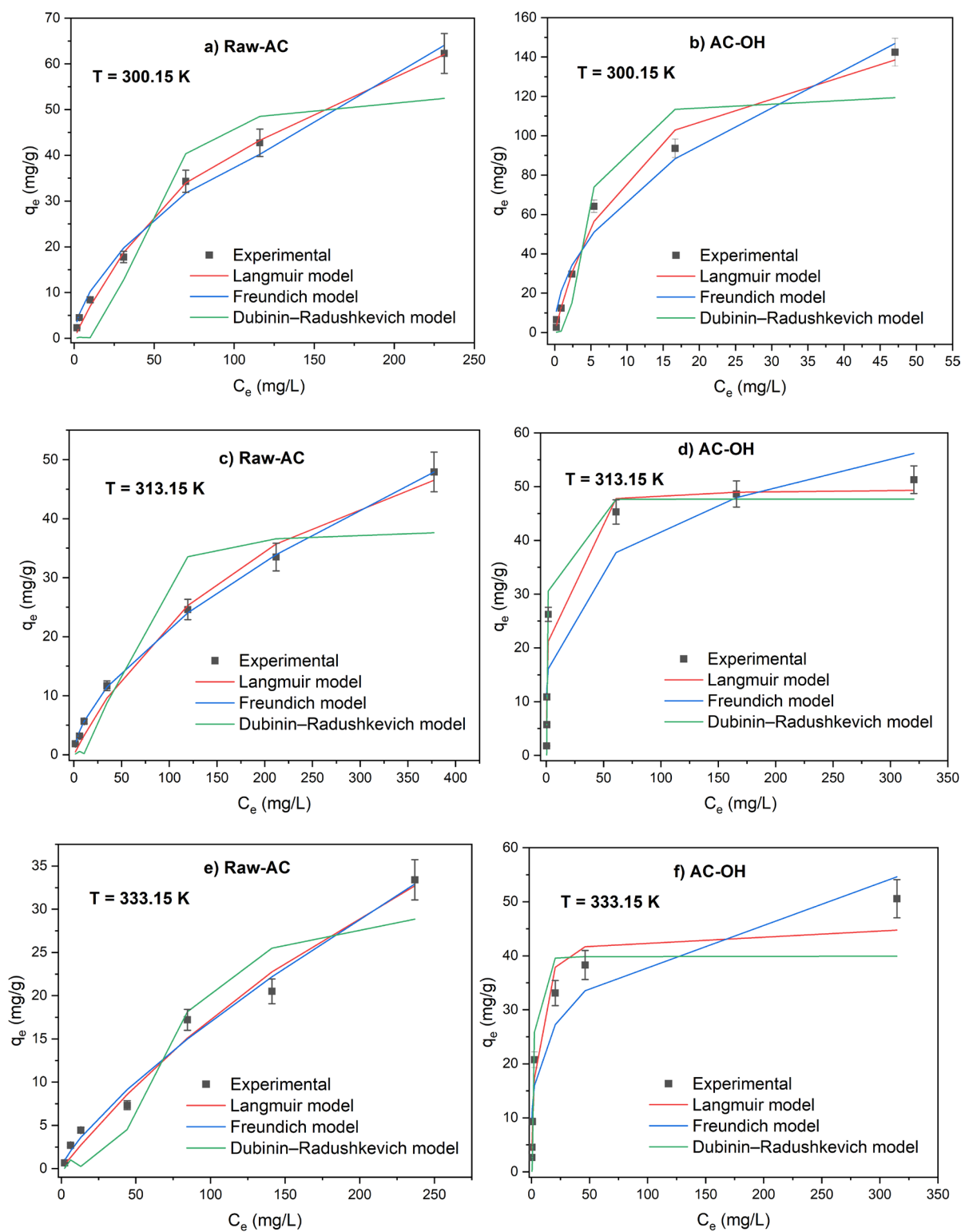


Figure 8. Adsorption isotherms of Pb(II) on Raw-AC and AC-OH at temperatures 300.15 (a,b), 313.15 (c,d), and 330.15 K (e,f).

The isotherm parameters were calculated using the nonlinear equations of Langmuir, Freundlich, and Dubinin–Radushkevich isotherm models.

As shown in Table 8, the adsorption of Pb(II) on AC-OH on the surface of different temperatures studied showed a best fitting to the Langmuir model, as indicated by the high correlation coefficient ($R^2 = 0.959\text{--}0.990$) when the temperature increased from 300.15 K to 330.15 K, the Langmuir constant Q_m of AC-OH, which indicates the monolayer saturation at equilibrium, decreased from 171.0 to 45.3 mg/g. In the case of Raw-AC, the adsorption of Pb(II) at ambient temperature showed a good fit to the Langmuir model, whereas at $T = 313.15$ and 330.15 K, it was best fitted to the Freundlich model and the values of K_F and n parameters decreased with the temperature rise. At all temperatures studied, the values of n parameters were between 1 and 10, indicating that AC-OH and Raw-AC favorably adsorb Pb(II) ions.

Table 8. Langmuir, Freundlich, and Dubinin–Radushkevich (D-R) isotherm parameters using nonlinear regression analysis for Pb(II) biosorption on Raw-AC and AC-OH biomass at different temperatures.

| Temperature (K) | Model | Parameters | Raw-AC | AC-OH |
|-----------------|----------------------------|------------------------------|---------|---------|
| 300.15 | Langmuir | Q_{\max} (mg/g) | 96.4 | 171 |
| | | $K_L \cdot 10^{-2}$ (L/mg) | 0.781 | 9.076 |
| | | R^2 | 0.997 | 0.990 |
| | Freundlich | K_F (mg/g)(L/mg) $^{1/n}$ | 2.654 | 22.311 |
| | | n | 1.71 | 2.043 |
| | | R^2 | 0.992 | 0.976 |
| | Dubinin–Radushkevich (D-R) | Q_{\max} (mg/g) | 53.840 | 120.205 |
| | | β (mol 2 /kJ 2) | 227.720 | 2.729 |
| | | E (kJ/mol) | 0.047 | 0.428 |
| R^2 | | 0.899 | 0.913 | |
| 313.15 | Langmuir | Q_{\max} (mg/g) | 76.1 | 49.6 |
| | | $K_L \cdot 10^{-2}$ (L/mg) | 0.417 | 42.48 |
| | | R^2 | 0.988 | 0.971 |
| | Freundlich | K_F (mg/g)(L/mg) $^{1/n}$ | 1.375 | 14.096 |
| | | n | 1.671 | 4.173 |
| | | R^2 | 0.999 | 0.884 |
| | Dubinin–Radushkevich (D-R) | Q_{\max} (mg/g) | 38.081 | 47.671 |
| | | β (mol 2 /kJ 2) | 264.046 | 0.324 |
| | | E (kJ/mol) | 0.044 | 1.243 |
| R^2 | | 0.865 | 0.970 | |
| 330.15 | Langmuir | Q_{\max} (mg/g) | 92.4 | 45.3 |
| | | $K_L \cdot 10^{-2}$ (L/mg) | 0.231 | 24.844 |
| | | R^2 | 0.981 | 0.959 |
| | Freundlich | K_F (mg/g)(L/mg) $^{1/n}$ | 0.508 | 12.635 |
| | | n | 1.311 | 3.329 |
| | | R^2 | 0.985 | 0.904 |
| | Dubinin–Radushkevich (D-R) | Q_{\max} (mg/g) | 30.879 | 39.923 |
| | | β (mol 2 /kJ 2) | 494.126 | 0.503 |
| | | E (kJ/mol) | 0.032 | 0.997 |
| R^2 | | 0.904 | 0.887 | |

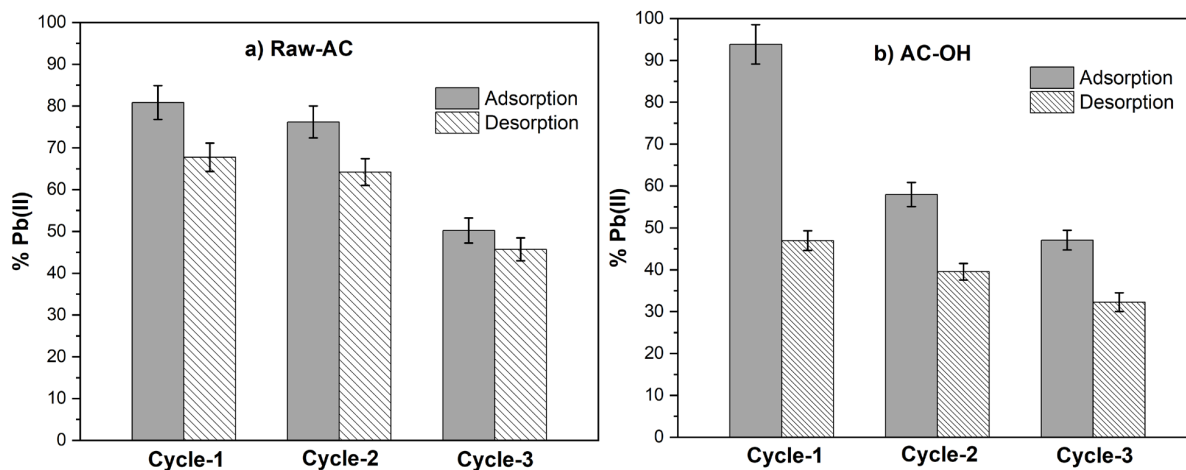
Error functions for all temperatures studied were calculated. Table 9 shows that for AC-OH, the Langmuir isotherms exhibit lower values of error functions for all temperatures studied and is a better fit compared with the Freundlich isotherm.

Table 9. Error function values of the Langmuir, Freundlich, and Dubinin–Radushkevich equilibrium models at 300.15, 313.15, and 330.15 K.

| Biosorbent | T (K) | Model | Error Functions | | | | | |
|------------|--------|------------|-----------------|----------|----------------|----------|--------|--------|
| | | | APE | SSE | $\Delta q(\%)$ | χ^2 | EABS | RMSE |
| Raw-AC | 300.15 | Langmuir | 19.583 | 9.119 | 0.303 | 3.133 | 6.721 | 1.350 |
| | | Freundlich | 20.027 | 20.996 | 0.291 | 1.405 | 11.534 | 2.049 |
| | | D-R | 52.451 | 298.240 | 70.076 | 608.200 | 42.590 | 7.723 |
| | 313.15 | Langmuir | 26.940 | 20.969 | 0.397 | 7.404 | 11.441 | 2.048 |
| | | Freundlich | 5.468 | 1.262 | 0.114 | 0.211 | 2.160 | 0.502 |
| | | D-R | 52.210 | 244.613 | 67.720 | 210.523 | 35.096 | 6.994 |
| | 330.15 | Langmuir | 23.035 | 16.390 | 0.305 | 3.404 | 9.584 | 1.811 |
| | | Freundlich | 18.858 | 12.375 | 0.242 | 1.310 | 7.947 | 1.573 |
| | | D-R | 47.879 | 75.587 | 63.686 | 94.235 | 19.872 | 3.888 |
| AC-OH | 300.15 | Langmuir | 16.701 | 169.569 | 0.218 | 4.109 | 25.363 | 5.824 |
| | | Freundlich | 81.765 | 402.405 | 1.312 | 16.084 | 48.817 | 8.971 |
| | | D-R | 55.163 | 1427.996 | 71.002 | 427.158 | 88.157 | 16.900 |
| | 313.15 | Langmuir | 54.847 | 80.379 | 1.131 | 7.002 | 20.212 | 4.009 |
| | | Freundlich | 102.467 | 317.822 | 2.177 | 19.917 | 40.802 | 7.973 |
| | | D-R | 37.865 | 97.503 | 57.454 | 78.557 | 23.568 | 4.416 |
| | 330.15 | Langmuir | 18.713 | 84.480 | 0.244 | 3.088 | 20.839 | 4.110 |
| | | Freundlich | 71.759 | 196.337 | 1.261 | 13.284 | 35.860 | 6.266 |
| | | D-R | 43.927 | 231.236 | 59.709 | 10.934 | 35.336 | 6.801 |

2.4. Adsorption and Desorption Study

Figures 9a and 9b show the adsorption and desorption cycles of Pb(II) on Raw-AC and AC-OH, respectively. It can be seen that after the three cycles, the percentage of Pb(II) removal on Raw-AC and AC-OH decreased from 80.82% to 45.70% and from 93.80% to 47.05%, respectively. Similarly, the Pb(II) desorption decreased from 67.75% to 45.70% and from 46.94% to 32.25% for Raw-AC and AC-OH, respectively. The decrease in the performance of adsorption and desorption of Raw-AC and AC-OH biosorbents was previously reported in other biosorbents, which was attributed to the possible remanent of metal ions on the surface of the biosorbent after the desorption step and the partial destruction of active functional groups by HCl after each regeneration cycle [22]. Despite the reduction in the percentage of Pb(II) removal after three cycles, both biosorbents have still shown efficient removal and desorption of Pb(II) after three times of recycling. As such, Raw-AC and AC-OH can be considered suitable recyclable biosorbents.

**Figure 9.** Adsorption and desorption cycles of Pb(II) with (a) Raw-AC and (b) AC-OH biosorbents.

2.5. Comparison of Natural and Alkali Ardisia Compressa K. with Other Biosorbents

In this study, the maximum Pb(II) biosorption capacity, according to Langmuir's model, was 96.4 and 170.9 mg/g using Raw-AC and AC-OH, respectively. As shown in Table 10, the results obtained in this work are within the usual values, and in some cases, they are between the highest maximum biosorption capacities for other similar biosorbents reported in the scientific literature, indicating the potential for its application in the removal of lead, and perhaps other heavy metals too, from contaminated effluents.

Table 10. Comparison of Pb(II) adsorption capacity of different sorbents.

| Biosorbent | Dose (g/L) | Ci (mg/L) | pH | Kinetic Model | Mechanism | $q_{e,max}$ (mg·g ⁻¹) | Ref. |
|--|---------------|-------------|---------|---------------|-----------------------|-----------------------------------|---------------|
| <i>Moringa oleifera</i> tree leaves | 4 | 20–200 | 5 | PSO | Chemisorption | 34.6 | [42] |
| <i>Nostoc commune</i> | 0.5 | 127–442 | 4.5–5.5 | PSO | Chemisorption | 384.6 | [28] |
| <i>Cystoseira stricta</i> | 1 | 0.5–1.0 | 3 | - | - | 65.0 | [50] |
| <i>Leucaena leucocephala</i> leaves | 10 | 10–500 | 6 | PSO | Chemisorption | 25.5 | [51] |
| <i>Ceratophyllum demersum</i> | 0.1 | 1.46–1.73 | 7 | - | Physical, monolayer | 44.8 | [52] |
| <i>Punica granatum</i> leaves | 0.1 | 1.46–1.73 | 7 | - | Physical, monolayer | 31.78 | [53] |
| <i>Mirabilis jalapa</i> leaves | 0.1 | 50–125 | 4.5 | - | Multimolecular layers | 38.5 | [54] |
| <i>Laurus nobilis</i> leaves waste | 4 | 5–10 | 6 | PFO | Chemisorption | 96.1 | [55] |
| <i>Cladophora fascicularis</i> | 2 | 225.4–838.3 | 5 | PSO | Chemisorption | 227.7 | [56] |
| Nickel ferrite nanoparticle | - | 0.01–0.05 | 5 | PSO | - | 19.2 | [57] |
| MoS ₂ /thiol-functionalized multiwalled carbon nanotube | 2 | 20–150 | 6 | PSO | Multilayer | 90.0 | [58] |
| Nano Zero-Valent Iron particles | 0.1 | 10–1000 | 6 | PSO | Chemisorption | 140.8 | [59] |
| Cu-Based Composite Track-Etched Membranes | 0.0033–0.0052 | 50 | 5 | PSO | Chemisorption | 0.44–0.56 | [60] |
| Raw-AC | 10 | 25–1000 | 6 | PSO | Chemisorption | 96.4 | In this study |
| AC-OH | 10 | 25–1000 | 6 | PSO | Chemisorption | 170.9 | In this study |

2.6. Proposed Mechanism of Interaction of Pb²⁺ with Raw-AC and AC-OH

The mechanism of interaction of Pb²⁺ with Raw-AC and AC-OH could be represented as shown in Figure 10 below:

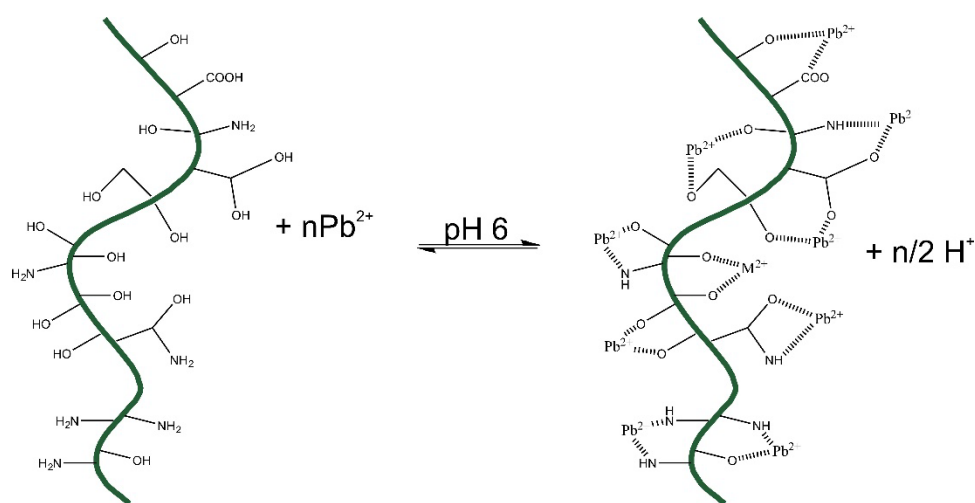


Figure 10. Interaction mechanism of the uptake of Pb²⁺ with raw-AC and AC-OH.

According to the FTIR results, both biomasses (Raw-AC and AC-OH) present, OH-, COOH, and NH₂ could be complexed with Pb²⁺ species, or some ion exchange could occur. Adjusting the pH to 4–6, the COOH groups of carboxylic acid release H⁺ into the solution.

This pH adjustment helps the complexation or electrostatic attraction of Pb^{2+} with both Raw-AC and AC-OH biomasses.

2.7. Data-Driven Optimization

An optimization study was conducted for the two materials (Raw-AC and AC-OH) and its objective was to find which type of material, along with its multivariate combination of initial concentration of Pb, mass, temperature, pH of the solution, and contact time, could provide the maximum q_e . However, optimization using the experimentation data required a couple of steps which are mentioned herewith:

1. In the first step: the original data was arranged in the form of a database (see Table 11), where all the tuning variables and the performance indicators were placed together. The database contained a total of 178 experimental points. Bringing the data in such a format would help in the development of an empirical model [61]. It was necessary to develop an empirical model because the optimization algorithms required a direct correlation between the tuning variables and the performance indicator. Thus, it was also necessary to understand the data through the heatmap of the Pearson coefficient of correlation (see Table 12) [62]. It was noted that the initial concentration of Pb was the variable with the highest level of sensitivity for q_e , and it was also noted that material 2 had a relatively higher tendency for higher values of q_e . The temperature and the pH of the solution were the least sensitive.

Table 11. Format of the database for the development of the empirical model. Note: material 1 refers to the combination of Raw-AC and material 2 refers to the combination of AC-OH.

| Material | Initial Concentration of Pb (mg/L) | Mass (g) | Temperature (K) | pH of the Solution | Contact Time (min) | q_e (mg/g) |
|----------|------------------------------------|----------|-----------------|--------------------|--------------------|--------------|
| 1 | 24.414 | 0.1 | 298.15 | 2 | 1440 | 2.41213 |
| 1 | 48.204 | 0.1 | 298.15 | 2 | 1440 | 4.33674 |
| 1 | 92.492 | 0.1 | 298.15 | 2 | 1440 | 7.1832 |
| 1 | 412.92 | 0.1 | 298.15 | 6 | 1440 | 34.3227 |
| 1 | 531.76 | 0.1 | 298.15 | 6 | 1440 | 41.574 |
| 1 | 854.16 | 0.1 | 298.15 | 6 | 1440 | 62.287 |
| 2 | 26.958 | 0.05 | 298.15 | 2 | 1440 | 5.36626 |
| 2 | 44.613 | 0.05 | 298.15 | 2 | 1440 | 8.84096 |
| 2 | 89.1 | 0.05 | 298.15 | 2 | 1440 | 17.61704 |
| 2 | 333.02 | 0.05 | 298.15 | 6 | 1440 | 63.7672 |
| 2 | 757.88 | 0.05 | 298.15 | 6 | 1440 | 127.848 |
| 2 | 1012.98 | 0.05 | 298.15 | 6 | 1440 | 147.475 |

Table 12. Understanding the correlation coefficient between the tuning and performance indicators through Pearson's coefficient of correlation.

| | Material | Initial Concentration of Pb | Mass | Temperature | pH of the Solution | Contact Time | q_e |
|-----------------------------|----------|-----------------------------|-------|-------------|--------------------|--------------|-------|
| Material | 1.00 | -0.01 | -0.24 | 0.01 | -0.01 | 0.01 | 0.27 |
| Initial concentration of Pb | -0.01 | 1.00 | 0.14 | -0.02 | -0.12 | 0.27 | 0.79 |
| Mass | -0.24 | 0.14 | 1.00 | -0.06 | 0.06 | 0.38 | -0.18 |
| Temperature | 0.01 | -0.02 | -0.06 | 1.00 | 0.16 | 0.22 | -0.03 |
| pH of the solution | -0.01 | -0.12 | 0.06 | 0.16 | 1.00 | -0.23 | -0.03 |
| Contact time | 0.01 | 0.27 | 0.38 | 0.22 | -0.23 | 1.00 | 0.22 |
| q_e | 0.27 | 0.79 | -0.18 | -0.03 | -0.03 | 0.22 | 1.00 |

2. In the second step, an empirical model was developed for the selected database. Such a model was developed through the application of artificial neural networks for regression models. The MATLAB environment using the nftool box was implemented.

All the input variables were placed in the input layer, and the performance indicator was placed in the performance indicator. A backpropagation method called Bayesian regularization backpropagation was implemented, which was suitable for the noisy database as the origin was experimentation [63]. The training, testing, and validation percentages were set to be 70, 15, and 15, respectively. The number of hidden neurons was iterated and a total of eight neurons came out to be optimal for the minimum mean square error. The regression fit and the error histogram are displayed in Figure 11. During the training, testing, and total phase, the values of R came out to be 0.99276, 0.977, and 0.9905, respectively, which indicates a high goodness of fit. The error histogram also fulfills the normality assumption of errors.

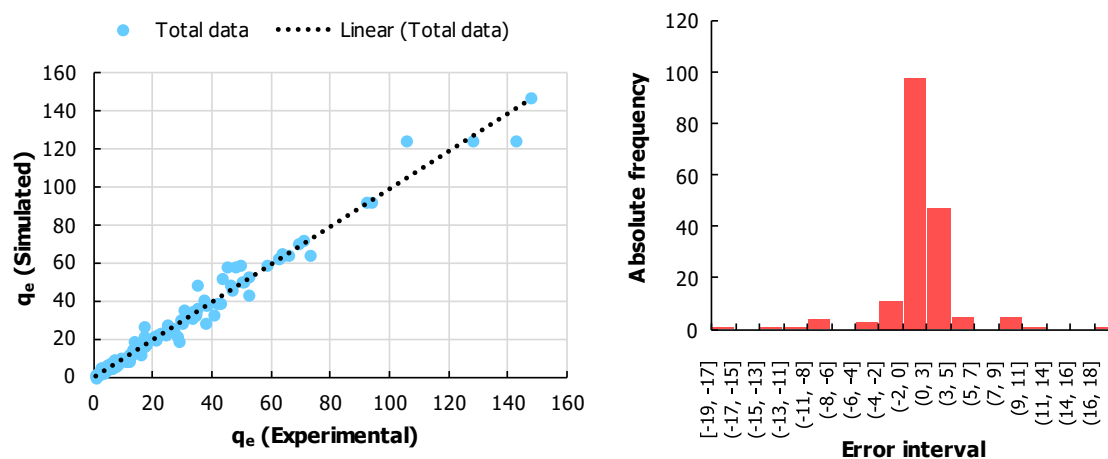


Figure 11. (Left) Results of empirical modeling through a comparison between experimental and simulated q_e . (Right) Histogram of the errors between the experimental and simulated q_e values.

- Once the empirical model was developed, in the last step, an optimization study could be conducted. The optimization study was conducted to maximize q_e for the given range of each of the tuning variables. The genetic algorithm was implemented in the MATLAB environment through its Optimization toolbox. All the generic configuration of the algorithm was taken to be default [64]. The optimization was conducted two times, one for each material, and the results are shown in Table 13. It is noted that the combination of tuning variables for each type of material was quite similar. For example, for Raw-AC, the optimal combination of temperature, pH of the solution, and contact time came out to be the same, which was 298.15 K, 6, and 1440 min, respectively. The only difference was noted in the cases of initial concentration of Pb and mass, which were 854.16 mg/L and 0.1 g for Raw-AC and 1012.98 mg/L and 0.05 g for AC-OH, respectively. It is quite interesting that even though a couple of variables were the same, the value of optimal q_e was quite different. For the combination of Raw-AC and AC-OH, the optimal q_e values came out to be 62.287 mg/g and 147.475 mg/g, respectively. It is remarkable how doing such a treatment can improve the results by 57.76%. It is also to be stressed here that the optimal point evaluated through the computational method was placed back into the experimental conditions and conformity between the optimal point through the computational method and the experimentation was met.

Table 13. Optimality of Raw-AC and AC-OH through conformity between the computational method and experimental procedure.

| Biomass | Initial Concentration of Pb (mg/L) | Mass (g) | Temperature (K) | pH of the Solution | Contact Time (min) | Optimal q_e (mg/g) |
|---------|------------------------------------|----------|-----------------|--------------------|--------------------|----------------------|
| Raw-AC | 854.16 | 0.1 | 298.15 | 6 | 1440 | 62.287 |
| AC-OH | 1012.98 | 0.05 | 298.15 | 6 | 1440 | 147.475 |

3. Materials and Methods

3.1. Pb standard Solutions

Stock solutions (1000 mg/L) of Pb(II) were prepared by dissolving 0.337 g of PbCl₂ (99%, Sigma Aldrich, St. Louis, MO, USA) in deionized water. Solutions with 25 to 700 mg/L concentrations were prepared by diluting the stock solutions using deionized water. Pb(II) calibration curves were obtained by diluting 1000 mg/L standard solutions of Pb in 2% v/v HNO₃ (Fluka Analytical, St. Louis, MO, USA).

3.2. Biosorbents

Leaves of *A. compressa* K. were manually collected from the experimental garden at Universidad Tecnológica de Xicotepec de Juárez, located in Xicotepec de Juárez, Puebla (−97.96 20° 16′ 33″ N, 97° 57′ 36″ W). Fresh leaves of *A. compressa* K. were washed, disinfected, and air-dried. The dry material was ground in a blender until a homogeneous fine powder (particle size between 0.42 and 0.80 mm) was obtained. The powder was preserved until use at room temperature in hermetically sealed plastic bags in the absence of light and humidity.

Alkali treatment of raw *A. compressa* K. (Raw-AC) was done as follows: 10 g of pulverized Raw-AC was added to 250 mL of 1.0 M NaOH in an Erlenmeyer flask (500 mL) and shaken at 140 rpm for 2 h. Then, the sample was filtered under a vacuum and rinsed several times using deionized water until the wash solution pH reached approximately 6.5. The treated biomass labeled AC-OH was air-dried and stored in glass bottles. Figure 12 illustrates the preparation procedure of the biosorbents.

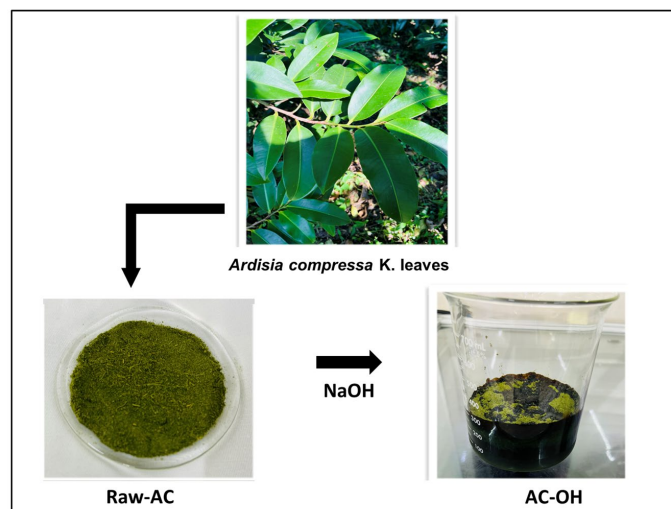


Figure 12. Schematic representation of the preparation of the biosorbents.

3.3. Physicochemical Analysis

Association of Analytical Communities (AOAC (2007)) methods were used for the chemical characterization of *A. compressa* leaves [65]: ash, moisture, raw fiber, and ethereal extract were found using the Soxhlet method; protein was found using the Kjeldahl method and nitrogen-free extract (NFE) was calculated using the percentage differences. The total soluble solids (TSSs) were identified using a digital refractometer (PR-101ATAGO PALETTE) according to the method previously described [65]. All determinations were done in triplicate.

3.4. Characterization Techniques

The pHPZC was obtained as previously described [32]. Samples of Raw-AC and AC-OH, before and after contact with metal ions, were characterized using a Fourier transform infrared spectrometer (Nicolet Nexus 670) to identify the functional groups on the biomass surface. Surface characteristics of Raw-AC and AC-OH biosorbents before and after the

uptake of Pb(II) were studied using scanning electron microscopy (JEOL JSM-IT300). An energy-dispersive X-ray spectrometer was used to determine the approximate chemical composition on the surface of Raw-AC and AC-OH biosorbents.

3.5. Biosorption Study

In this work, the biosorption process was carried out using a batch technique. For the kinetic study, 0.1 g of Raw-AC and AC-OH was mixed with 10 mL of Pb(II) solutions at initial concentrations from 25 mg/L to 250 mg/L. The samples were shaken at 140 rpm in an orbital shaker (CRP-0228, Scientific) for times ranging from 15 min to 1440 min. After each contact time, the samples were centrifuged (CRM Globe, Certificient, Chicago, IL, USA) for 5 min, and the Pb(II) contents in the aqueous solutions were determined using flame atomic absorption spectrometry (iCe Serie TermoScientific).

After each contact time, the amount of Pb(II) adsorbed on the surface of Raw-AC and AC-OH was calculated using Equation (1):

$$q_t = \frac{C_i - C_t}{m} \cdot V \quad (1)$$

where C_i and C_t are, respectively, the initial and final concentrations of Pb(II) (mg/L); V (L) is the volume of solution; and m (g) is the mass of biosorbents.

In this study, the effects of the solution pH, dose of the biosorbents, and temperature were carried out by varying the initial lead concentration from 25 to 1000 mg/L. For the kinetic study, the temperature and solution pH were fixed, whereas the initial lead concentration was varied from 25 to 250 mg/L and the contact time was changed from 5 to 1440 min.

Table 14 gives the experimental conditions used to investigate the effects of contact times, solution pH, temperature, and dose of biosorbents on the removal of Pb(II).

Table 14. Values of contact times, solution pH, temperature, and adsorbent dose parameters used for the experimental process.

| Experiments | Experimental Parameters | | | | |
|---------------|-------------------------|------------|-----------------------|------------|-----------------|
| | pH | Time (min) | C _i (mg/L) | Dose (g/L) | Temperature (K) |
| Solution pH | 2–6 | 1440 | 25–1000 | 10 | 300.15 |
| Dose | 6 | 1440 | 25–1000 | 5–20 | 300.15 |
| Contact times | 6 | 5–1440 | 25–250 | 10 | 300.15 |
| Temperature | 6 | 1440 | 25–1000 | 10 | 300.15–330.15 |

All experiments were performed in duplicate and the results were expressed as averaged values. The Supplementary Materials provide the kinetic and isotherm models, as well as the error functions analysis used in this study.

3.6. Kinetic Models

This study employed the nonlinear equations of pseudo-first- and pseudo-second-order models (Equation (2) and Equation (3), respectively) to investigate the kinetics of Pb(II) biosorption onto Raw-AC and AC-OH:

$$q_t = q_e(1 - \exp(-k_1 t)) \quad (2)$$

$$q_t = \frac{k_2 q_e^2 t}{1 + k_2 q_e t} \quad (3)$$

where q_e is the theoretical adsorption capacity (mg/g), and k_1 (1/min) and k_2 (g/mg min) are the pseudo-first- and pseudo-second-order rate constants, respectively.

3.7. Isotherm Models

Experimental data were examined using Langmuir, Freundlich, and Dubinin-Radushkevich (D-R) isotherm models.

Equation (4) describes the non-linear form of the Langmuir isotherm model:

$$q_e = \frac{q_m K_L C_e}{1 + K_L C_e} \quad (4)$$

where q_m (mg/g) is the maximum sorption capacity, and K_L (L/mg) is the Langmuir equilibrium constant, which indicates the affinity of the sorbate for the solute [55].

The Langmuir model assumes that adsorption takes place for monolayer adsorption of the adsorbate from a liquid solution on a surface of biosorbent containing a finite number of identical sites and all adsorption sites have equal adsorption energies [55,66].

The Freundlich model is an empirical isotherm that can be used for non-ideal adsorption, which is mostly used to understand the adsorption of metal ions on a heterogeneous surface with multilayer adsorption. It can also define an exponential distribution of active sites and their energy [54]. The non-linear form of the Freundlich isotherm model is expressed as Equation (5):

$$q_e = K_F C_e^{1/n} \quad (5)$$

where K_F (mg/g)(L/mg)^{1/n} and n are the Freundlich constants associated with the adsorption capacity and adsorption intensity of the adsorbent, respectively. C_e (mg/L) is the adsorbate equilibrium concentration. When $n = 1$, the isotherm is linear and indicates that all sites on the adsorbent have equal affinity for the adsorbates. Values of $n > 1$ indicate the affinities decreased with increasing adsorption density [54]. The greater the value of n , the more favorable the adsorption and the more heterogeneous the surface of the particles will be [67].

The D-R isotherm is an empirical model that is generally employed to find whether the adsorption involved in the experimental data is physical or chemical [68]. The non-linear form of the D-R isotherm model is shown in the following Equation (6):

$$q_e = q_m e^{-\beta \epsilon^2} \quad (6)$$

where β (mol²/kJ²) is a constant related to adsorption energy, $\epsilon = RT \ln \left(1 + \frac{1}{C_e}\right)$ is the adsorption potential (kJ mol⁻¹), R (8.314 J mol⁻¹ K⁻¹) is the universal gas constant, T (K) is the absolute temperature, and $E = \frac{1}{\sqrt{2\beta}}$ is the adsorption energy (kJ/mol).

The numerical value from the free energy of the molecule (E) gives an indication of the nature of the interaction forces between lead ions and the active sites on the composite surface. When the value of the adsorption energy was less than 8 kJ/mol, it indicates that the adsorption occurred physically; if it was between 8 and 16 kJ/mol, it suggests that the adsorption process was carried out chemically, driven by the ion exchange mechanism; and chemisorption was observed when E values are between 20 and 40 kJ/mol [69].

3.8. Adsorption–Desorption Cycles

Experiments of adsorption and desorption cycles were conducted: 10 g/L of Raw-AC and AC-OH were mixed with 1000 mg/L of Pb(II) for 1440 min at room temperature and solution pH at 6. The samples were filtered, and the adsorption efficiency was obtained utilizing Equation (7):

$$\text{Adsorption efficiency \%} = \frac{C_{ads}}{C_{initial}} \times 100 \quad (7)$$

After the adsorption process, the biosorbents were dried and weighed; then, the desorption experiments were conducted by mixing the biosorbents at ambient temperature

for 2 h with 0.5 M HCl. The Pb(II) concentrations in each solution were measured, and the desorption efficiency was obtained utilizing Equation (8):

$$\text{Desorption efficiency \%} = \frac{C_{des}}{C_{ads}} \times 100 \quad (8)$$

where C_{des} is the concentration of Pb(II) desorbed in mg/g and C_{ads} is the concentration of Pb(II) adsorbed in mg/g.

After desorption, the samples were rinsed several times with deionized water to remove the eluent agent from the biosorbents. The samples were then dried and weighed for further reuse. In this study, three adsorption and desorption cycles were repeated.

3.9. Framework of Empirical Model and Optimization Process

Owing to the complexity of the involvement of so many tuning variables, it is not easy to determine the optimal set conditions for this problem. For this purpose, an artificial intelligence method consisting of the artificial neural network was adapted for the empirical modeling, and later on, a genetic algorithm was applied for optimization purposes, which would eventually give out the best combination of all the multivariate tuning variables [70].

4. Conclusions

In conclusion, this study demonstrates that *Ardisia compressa* K. leaves, particularly those treated with a solution of 1M NaOH (AC-OH), exhibit a higher sorption capacity for Pb(II) from aqueous solutions compared with natural *Ardisia compressa* K. leaves (Raw-AC). The surface modification of the biosorbent after the alkali treatment was confirmed via pH_{PZC} and FTIR analysis, which revealed the presence of carboxyl, hydroxyl, and amino groups responsible for Pb(II) binding.

The removal of Pb(II) was found to be dependent on various factors, including solution pH, contact time, biosorbent dose, and water temperature. The optimum experimental conditions for maximum Pb(II) removal by both biosorbents were at pH 6 and T = 300.15 K.

The kinetic data analysis indicated that the pseudo-second-order kinetic model best described Pb(II) biosorption on both Raw-AC and AC-OH, which suggests that chemisorption controlled the rate of reaction. The Langmuir isotherm model described the adsorption isotherms for both biosorbents at different solution pH values well, suggesting monolayer sorption on a homogeneous surface took place. Furthermore, the study introduced the application of artificial neural networks and genetic algorithms for regression modeling and optimization purposes.

The model showed high reliability, and the optimization study revealed a significant improvement of around 57.76% in the indicator “ q_e ” for AC-OH. The optimal conditions for AC-OH were determined as follows: initial concentration of Pb: 1012.98 mg/L, mass: 0.05 g, temperature: 298.15 K, pH of the solution: 6, and contact time: 1440 min, resulting in an optimal q_e of 147.475 mg/g. In summary, the results indicate that *Ardisia compressa* K. leaves can serve as a promising, cost-effective, and efficient biosorbent for removing Pb(II) ions from aqueous solutions. The study also highlights the potential of artificial neural networks and genetic algorithms for optimizing biosorption processes. These findings contribute to the development of environmentally friendly and sustainable methods for heavy metal removal from water sources.

A significant finding of this study pertains to the coefficient of determination, which indicated that the Dubinin–Radushkevich isotherm model exhibited lower values compared with the Langmuir and Freundlich, suggesting a need for further investigation into the applicability and parameter-based assessment of the Dubinin–Radushkevich model to elucidate sorption mechanisms.

The insights from this research hold valuable implications for engineering education, as it showcases how modifying biosorbents, optimizing process conditions, employing kinetic and isotherm models, and utilizing advanced techniques like artificial neural networks and genetic algorithms can be integrated into engineering curricula to foster a

comprehensive understanding of designing effective and eco-friendly solutions for heavy metal removal in water treatment systems. The social insights derived from this research underscore the potential impact of innovative engineering approaches on addressing environmental challenges, demonstrating the significance of interdisciplinary collaboration between engineering and environmental sciences to develop sustainable solutions for water pollution, thereby imparting the importance of considering broader societal and ecological implications of technological advancements in engineering education.

Supplementary Materials: The following supporting information can be downloaded from <https://www.mdpi.com/article/10.3390/molecules28176387/s1>. Error functions analysis.

Author Contributions: A.Y.V.-S., M.A. and A.A.S. conceived and planned the experiments; A.A.S., C.A. and I.A. contributed to the characterization of the samples. M.A., R.T. and A.R.V.-O. wrote the manuscript with input from all authors. E.C.L., M.A. and I.A. contributed to the interpretation of the results. All authors provided critical feedback and helped to shape the research, analysis, and manuscript. All authors have read and agreed to the published version of the manuscript.

Funding: This research received no external funding.

Institutional Review Board Statement: Not applicable.

Informed Consent Statement: Not applicable.

Data Availability Statement: The data presented in this study are available on request from the corresponding author.

Acknowledgments: The authors are grateful to Adriana Tejada Cruz and Eliezer Hernández Me-cinas for their assistance in the X-ray diffraction and FTIR measurements.

Conflicts of Interest: The authors declare no conflict of interest.

Sample Availability: Not applicable.

References

1. Kinuthia, G.K.; Ngure, V.; Beti, D.; Lugalia, R.; Wangila, A.; Kamau, L. Levels of heavy metals in wastewater and soil samples from open drainage channels in Nairobi, Kenya: Community health implication. *Sci. Rep.* **2020**, *10*, 8434. [[CrossRef](#)]
2. Ben Omar, M.; Mendiguchía, C.; Er-Raioui, H.; Marhraoui, M.; Lafraoui, G.; Oulad-Abdellah, M.K.; García-Vargas, M.; Moreno, C. Distribution of heavy metals in marine sediments of Tetouan coast (North of Morocco): Natural and anthropogenic sources. *Environ. Earth Sci.* **2015**, *74*, 4171–4185. [[CrossRef](#)]
3. Mendiguchía, C.; Moreno, C.; García-Vargas, M. Evaluation of natural and anthropogenic influences on the Guadalquivir River (Spain) by dissolved heavy metals and nutrients. *Chemosphere* **2007**, *69*, 1509–1517. [[CrossRef](#)] [[PubMed](#)]
4. Sandeep, G.; Vijayalatha, K.R.; Anitha, T. Heavy metals and its impact in vegetable crops. *Int. J. Chem. Stud.* **2019**, *7*, 1612–1621.
5. Vajargah, M.F. A Review on the Effects of Heavy Metals on Aquatic Animals. *J. Biomed. Res. Environ. Sci.* **2021**, *2*, 865–869. [[CrossRef](#)]
6. Munir, N.; Jahangeer, M.; Bouyahya, A.; El Omari, N.; Ghchime, R.; Balahbib, A.; Aboulaghras, S.; Mahmood, Z.; Akram, M.; Shah, S.M.A.; et al. Heavy metal contamination of natural foods is a serious health issue: A review. *Sustainability* **2022**, *14*, 161. [[CrossRef](#)]
7. Vievard, J.; Alem, A.; Pantet, A.; Ahfir, N.-D.; Arellano-Sánchez, M.G.; Devouge-Boyer, C.; Mignot, M. Bio-Based Adsorption as Ecofriendly Method for Wastewater Decontamination: A Review. *Toxics* **2023**, *11*, 404. [[CrossRef](#)]
8. Rajendran, S.; Priya, A.K.; Kumar, P.S.; Hoang, T.K.; Sekar, K.; Chong, K.Y.; Khoo, K.S.; Ng, H.S.; Show, P.L. A critical and recent developments on adsorption technique for removal of heavy metals from wastewater—A review. *Chemosphere* **2022**, *303*, 135146. [[CrossRef](#)]
9. Pandey, P.K.; Sharma, S.K.; Sambhi, S.S. Removal of lead(II) from waste water on zeolite-NaX. *J. Environ. Chem. Eng.* **2015**, *3*, 2604–2610. [[CrossRef](#)]
10. Uddin, M.K. A review on the adsorption of heavy metals by clay minerals, with special focus on the past decade. *Chem. Eng. J.* **2017**, *308*, 438–462. [[CrossRef](#)]
11. Nordin, N.A.; Rahman, N.A.; Abdullah, A.H. Effective Removal of Pb(II) Ions by Electrospun PAN/Sago Lignin-Based Activated Carbon Nanofibers. *Molecules* **2020**, *25*, 3081. [[CrossRef](#)] [[PubMed](#)]
12. Nguyen, T.; Ngo, H.; Guo, W.; Zhang, J.; Liang, S.; Yue, Q.; Li, Q. Applicability of agricultural waste and by-products for adsorptive removal of heavy metals from wastewater. *Bioresour. Technol.* **2013**, *148*, 574–585. [[CrossRef](#)]
13. Ge, Y.; Qin, L.; Li, Z. Lignin microspheres: An effective and recyclable natural polymer-based adsorbent for lead ion removal. *Mater. Des.* **2016**, *95*, 141–147. [[CrossRef](#)]

14. Chakraborty, R.; Asthana, A.; Singh, A.K.; Jain, B.; Susan, A.B.H. Adsorption of heavy metal ions by various low-cost adsorbents: A review. *Int. J. Environ. Anal. Chem.* **2022**, *102*, 342–379. [[CrossRef](#)]
15. Hegazi, H.A. Removal of heavy metals from wastewater using agricultural and industrial wastes as adsorbents. *HBRC J.* **2013**, *9*, 276–282. [[CrossRef](#)]
16. Joseph, L.; Jun, B.M.; Flora, J.R.V.; Park, C.M.; Yoon, Y. Removal of heavy metals from water sources in the developing world using low-cost materials: A review. *Chemosphere* **2019**, *229*, 142–159. [[CrossRef](#)]
17. Demirbas, A. Heavy metal adsorption onto agro-based waste materials: A review. *J. Hazard. Mater.* **2008**, *157*, 220–229. [[CrossRef](#)]
18. Elkhaleefa, A.; Ali, I.H.; Brima, E.I.; Shigidi, I.; Elhag, A.B.; Karama, B. Evaluation of the adsorption efficiency on the removal of lead(II) ions from aqueous solutions using *Azadirachta indica* leaves as an adsorbent. *Processes* **2021**, *9*, 559. [[CrossRef](#)]
19. Jayasree, R.; Kumar, P.S.; Saravanan, A.; Hemavathy, R.; Yaashikaa, P.; Arthi, P.; Shreshta, J.; Jeevanantham, S.; Karishma, S.; Arasu, M.V.; et al. Sequestration of toxic Pb(II) ions using ultrasonic modified agro waste: Adsorption mechanism and modelling study. *Chemosphere* **2021**, *285*, 131502. [[CrossRef](#)]
20. Zhang, Z.; Wang, T.; Zhang, H.; Liu, Y.; Xing, B. Adsorption of Pb(II) and Cd(II) by magnetic activated carbon and its mechanism. *Sci. Total Environ.* **2021**, *757*, 143910. [[CrossRef](#)]
21. Saleh Al-Hashemi, Z.S.; Hossain, M.A. Biological activities of different neem leaf crude extracts used locally in Ayurvedic medicine. *Pac. Sci. Rev. A Nat. Sci. Eng.* **2016**, *18*, 128–131. [[CrossRef](#)]
22. Tran, H.N.; Chao, H.P. Adsorption and desorption of potentially toxic metals on modified biosorbents through new green grafting process. *Environ. Sci. Pollut. Res.* **2018**, *25*, 12808–12820. [[CrossRef](#)] [[PubMed](#)]
23. Joaquín-Cruz, E.; Dueñas, M.; García-Cruz, L.; Salinas-Moreno, Y.; Santos-Buelga, C.; García-Salinas, C. Anthocyanin and phenolic characterization, chemical composition and antioxidant activity of chagalapoli (*Ardisia compressa* K.) fruit: A tropical source of natural pigments. *Food Res. Int.* **2015**, *70*, 151–157. [[CrossRef](#)]
24. Vázquez-Sánchez, A.Y.; Corfield, R.; Sosa, N.; Salvatori, D.; Schebor, C. Physicochemical, functional, and sensory characterization of apple leathers enriched with acáchul (*Ardisia compressa* Kunth) powder. *LWT* **2021**, *146*, 111472. [[CrossRef](#)]
25. Chandra, S.; De Mejia, E.G. Polyphenolic compounds, antioxidant capacity, and quinone reductase activity of an aqueous extract of *Ardisia compressa* in comparison to mate (*Ilex paraguariensis*) and green (*Camellia sinensis*) teas. *J. Agric. Food Chem.* **2004**, *52*, 3583–3589. [[CrossRef](#)] [[PubMed](#)]
26. Thamaga, M.W.; Mokoboki, H.K.; Sebola, N.A.; Ravhuhali, K.E. Apparent digestibility and nutritional composition of *Leucaena leucocephala* (Lam) leaf meal incorporated in the diets of Black Australorp and Potchefstroom Koekoek chicken breeds. *Trop. Anim. Health Prod.* **2021**, *53*, 458. [[CrossRef](#)] [[PubMed](#)]
27. Garcia, G.W.; Ferguson, T.U.; Neckles, F.A.; Archibald, K.A.E. The nutritive value and forage productivity of *Leucaena leucocephala*. *Anim. Feed. Sci. Technol.* **1996**, *60*, 29–41. [[CrossRef](#)]
28. Lavado-Meza, C.; De la Cruz-Cerrón, L.; Lavado-Puente, C.; Angeles-Suazo, J.; Dávalos-Prado, J.Z. Efficient Lead Pb(II) Removal with Chemically Modified Nostoc commune Biomass. *Molecules* **2023**, *28*, 268. [[CrossRef](#)] [[PubMed](#)]
29. Ayssiwede, S.B.; Dieng, A.; Chrysostome, C.; Ossebi, W.; Hornick, J.L.; Missouhou, A. Digestibility, metabolic utilization and nutritional value of *Leucaena leucocephala* (Lam.) leaf meal incorporated in indigenous Senegal chickens diets. *Adv. Anim. Biosci.* **2010**, *1*, 425–426. [[CrossRef](#)]
30. Torres-Maza, A.; Yupanqui-Bacilio, C.; Castro, V.; Aguirre, E.; Villanueva, E.; Rodríguez, G. Comparison of the hydrocolloids *Nostoc commune* and *Nostoc sphaericum*: Drying, spectroscopy, rheology and application in nectar. *Sci. Agropecu.* **2020**, *11*, 583–589. [[CrossRef](#)]
31. Šoštarić, T.D.; Petrović, M.S.; Pastor, F.T.; Lončarević, D.R.; Petrović, J.T.; Milojković, J.V.; Stojanović, M.D. Study of heavy metals biosorption on native and alkali-treated apricot shells and its application in wastewater treatment. *J. Mol. Liq.* **2018**, *259*, 340–349. [[CrossRef](#)]
32. Abatal, M.; Lima, E.C.; Anastopoulos, I.; Giannakoudakis, D.A.; Vargas, J.; Aguilar, C.; Olguín, M.; Anguebes-Fransechi, F. Effect of alkali treatment on the removal of Co(II) ions by *Leucaena leucocephala* biomass. *J. Mol. Liq.* **2022**, *367*, 120419. [[CrossRef](#)]
33. Fernandez, M.E.; Nunell, G.V.; Bonelli, P.R.; Cukierman, A.L. Batch and dynamic biosorption of basic dyes from binary solutions by alkaline-treated cypress cone chips. *Bioresour. Technol.* **2012**, *106*, 55–62. [[CrossRef](#)] [[PubMed](#)]
34. Farnane, M.; Tounsadi, H.; Elmoubarki, R.; Mahjoubi, F.; Elhalil, A.; Saqrane, S.; Abdennouri, M.; Qourzal, S.; Barka, N. Alkaline treated carob shells as sustainable biosorbent for clean recovery of heavy metals: Kinetics, equilibrium, ions interference and process optimisation. *Ecol. Eng.* **2017**, *101*, 9–20. [[CrossRef](#)]
35. Bayramoğlu, G.; Çelik, G.; Arica, M.Y. Biosorption of Reactive Blue 4 dye by native and treated fungus *Phanerocheate chrysosporium*: Batch and continuous flow system studies. *J. Hazard. Mater.* **2006**, *137*, 1689–1697. [[CrossRef](#)] [[PubMed](#)]
36. Chen, G.Q.; Zeng, G.M.; Tu, X.; Niu, C.G.; Huang, G.H.; Jiang, W. Application of a by-product of *Lentinus edodes* to the bioremediation of chromate contaminated water. *J. Hazard. Mater.* **2006**, *135*, 249–255. [[CrossRef](#)] [[PubMed](#)]
37. Rezaei, M.; Pourang, N.; Moradi, A.M. Removal of lead from aqueous solutions using three biosorbents of aquatic origin with the emphasis on the affective factors. *Sci. Rep.* **2022**, *12*, 751. [[CrossRef](#)] [[PubMed](#)]
38. Bhattacharya, P.; Mallick, K.; Ghosh, S.; Banerjee, P.; Mukhopadhyay, A.; Bandyopadhyay, S. Algal biomass as potential biosorbent for reduction of organic load in gray water and subsequent reuse: Effect on seed germination and enzyme activity. *Bioremediat. J.* **2014**, *18*, 56–70. [[CrossRef](#)]

39. Faghihian, H.; Peyvandi, S. Adsorption isotherm for uranyl biosorption by *Saccharomyces cerevisiae* biomass. *J. Radioanal. Nucl. Chem.* **2012**, *293*, 463–468. [[CrossRef](#)]
40. Aksu, Z.; Açıkel, Ü.; Kabasakal, E.; Tezer, S. Equilibrium modelling of individual and simultaneous biosorption of chromium(VI) and nickel(II) onto dried activated sludge. *Water Res.* **2002**, *36*, 3063–3073. [[CrossRef](#)]
41. Huang, Y.; Li, S.; Chen, J.; Zhang, X.; Chen, Y. Adsorption of Pb(II) on mesoporous activated carbons fabricated from water hyacinth using H₃PO₄ activation: Adsorption capacity, kinetic and isotherm studies. *Appl. Surf. Sci.* **2014**, *293*, 160–168. [[CrossRef](#)]
42. Reddy, D.H.K.; Seshaiha, K.; Reddy, A.; Rao, M.M.; Wang, M.C. Biosorption of Pb²⁺ from aqueous solutions by *Moringa oleifera* bark: Equilibrium and kinetic studies. *J. Hazard. Mater.* **2010**, *174*, 831–838. [[CrossRef](#)] [[PubMed](#)]
43. Yuvaraja, G.; Krishnaiah, N.; Subbaiah, M.V.; Krishnaiah, A. Biosorption of Pb(II) from aqueous solution by *Solanum melongena* leaf powder as a low-cost biosorbent prepared from agricultural waste. *Colloids Surf. B Biointerfaces* **2014**, *114*, 75–81. [[CrossRef](#)] [[PubMed](#)]
44. Patel, R.; Suresh, S. Kinetic and equilibrium studies on the biosorption of reactive black 5 dye by *Aspergillus foetidus*. *Bioresour. Technol.* **2008**, *99*, 51–58. [[CrossRef](#)] [[PubMed](#)]
45. Bhattacharyya, K.G.; Gupta, S.S. Adsorptive accumulation of Cd(II), Co(II), Cu(II), Pb(II), and Ni(II) from water on montmorillonite: Influence of acid activation. *J. Colloid. Interface Sci.* **2007**, *310*, 411–424. [[CrossRef](#)] [[PubMed](#)]
46. Alsohaimi, I.H.; Wabaidur, S.M.; Kumar, M.; Khan, M.A.; Alothman, Z.A.; Abdalla, M.A. Synthesis, characterization of PMDA/TMSPEDA hybrid nano-composite and its applications as an adsorbent for the removal of bivalent heavy metals ions. *Chem. Eng. J.* **2015**, *270*, 9–21. [[CrossRef](#)]
47. Bhattacharyya, K.G.; Sharma, A. Adsorption of Pb(II) from aqueous solution by *Azadirachta indica* (Neem) leaf powder. *J. Hazard. Mater.* **2004**, *113*, 97–109. [[CrossRef](#)] [[PubMed](#)]
48. Kumar, K.V.; Sivanesan, S. Prediction of optimum sorption isotherm: Comparison of linear and non-linear method. *J. Hazard. Mater.* **2005**, *126*, 198–201. [[CrossRef](#)]
49. Mondal, M.K. Removal of Pb(II) from aqueous solution by adsorption using activated tea waste. *Korean J. Chem. Eng.* **2010**, *27*, 144–151. [[CrossRef](#)]
50. Iddou, A.; Hadj Youcef, M.; Aziz, A.; Ouali, M.S. Biosorptive removal of lead (II) ions from aqueous solutions using *Cystoseira stricta* biomass: Study of the surface modification effect. *J. Saudi Chem. Soc.* **2011**, *15*, 83–88. [[CrossRef](#)]
51. Cimá-Mukul, C.A.; Abdellaoui, Y.; Abatal, M.; Vargas, J.; Santiago, A.A.; Barrón-Zambrano, J.A. Eco-Efficient Biosorbent Based on *Leucaena leucocephala* Residues for the Simultaneous Removal of Pb (II) and Cd (II) Ions from Water System: Sorption and Mechanism. *Bioinorg. Chem. Appl.* **2019**, *2019*, 2814047. [[CrossRef](#)]
52. Keskinan, O.; Goksu, M.Z.L.; Basibuyuk, M.; Forster, C.F. Heavy metal adsorption properties of a submerged aquatic plant (*Ceratophyllum demersum*). *Bioresour. Technol.* **2004**, *92*, 197–200. [[CrossRef](#)] [[PubMed](#)]
53. Salehi, P.; Asghari, B.; Mohammadi, F. Biosorption of Ni(II), Cu(II) and Pb(II) by *Punica granatum* from Aqueous Solutions. *J. Water Resour. Prot.* **2010**, *2*, 701–705. [[CrossRef](#)]
54. Begum, S.A.S.; Tharakeswar, Y.; Kalyan, Y.; Naidu, G.R. Biosorption of Cd (II), Cr (VI) & Pb (II) from Aqueous Solution Using *Mirabilis jalapa* as Adsorbent. *J. Encapsulation Adsorpt. Sci.* **2015**, *5*, 93–104. [[CrossRef](#)]
55. Gümüş, D. Biosorptive application of defatted *Laurus nobilis* leaves as a waste material for treatment of water contaminated with heavy metal. *Int. J. Phytoremediation* **2019**, *21*, 556–563. [[CrossRef](#)]
56. Deng, L.; Su, Y.; Su, H.; Wang, X.; Zhu, X. Sorption and desorption of lead (II) from wastewater by green algae *Cladophora fascicularis*. *J. Hazard. Mater.* **2007**, *143*, 220–225. [[CrossRef](#)] [[PubMed](#)]
57. Khoso, W.A.; Haleem, N.; Baig, M.A.; Jamal, Y. Synthesis, characterization and heavy metal removal efficiency of nickel ferrite nanoparticles (NFN's). *Sci. Rep.* **2021**, *11*, 3790. [[CrossRef](#)]
58. Gusain, R.; Kumar, N.; Fosso-Kankeu, E.; Ray, S.S. Efficient Removal of Pb(II) and Cd(II) from Industrial Mine Water by a Hierarchical MoS₂/SH-MWCNT Nanocomposite. *ACS Omega* **2019**, *4*, 13922–13935. [[CrossRef](#)] [[PubMed](#)]
59. Sepehri, S.; Kanani, E.; Abdoli, S.; Rajput, V.D.; Minkina, T.; Lajayer, B.A. Pb(II) Removal from Aqueous Solutions by Adsorption on Stabilized Zero-Valent Iron Nanoparticles—A Green Approach. *Water* **2023**, *15*, 222. [[CrossRef](#)]
60. Altynbaeva, L.S.; Mashentseva, A.A.; Aimanova, N.A.; Zheltov, D.A.; Shlimas, D.I.; Nurpeisova, D.T.; Barsbay, M.; Abuova, F.U.; Zdorovets, M.V. Eco-Friendly Electroless Template Synthesis of Cu-Based Composite Track-Etched Membranes for Sorption Removal of Lead(II) Ions. *Membranes* **2023**, *13*, 495. [[CrossRef](#)] [[PubMed](#)]
61. Tariq, R.; Ali, M.; Sheikh, N.A.; Shahzad, M.W.; Xu, B.B. Deep learning artificial intelligence framework for sustainable desiccant air conditioning system: Optimization towards reduction in water footprints. *Int. Commun. Heat Mass Transf.* **2023**, *140*, 106538. [[CrossRef](#)]
62. Tariq, R.; Torres-Aguilar, C.E.; Xamán, J.; Zavala-Guillén, I.; Bassam, A.; Ricalde, L.J.; Carvente, O. Digital twin models for optimization and global projection of building-integrated solar chimney. *Build. Environ.* **2022**, *213*, 108807. [[CrossRef](#)]
63. Tariq, R.; Cetina-Quiñones, A.J.; Cardoso-Fernández, V.; Daniela-Abigail, H.L.; Soberanis, M.A.E.; Bassam, A.; De Lille, M.V. Artificial intelligence assisted technoeconomic optimization scenarios of hybrid energy systems for water management of an isolated community. *Sustain. Energy Technol. Assess.* **2021**, *48*, 101561. [[CrossRef](#)]
64. Tariq, R.; Abatal, M.; Bassam, A. Computational intelligence for empirical modeling and optimization of methylene blue adsorption phenomena using available local zeolites and clay of Morocco. *J. Clean. Prod.* **2022**, *370*, 133517. [[CrossRef](#)]

65. Vicente-Flores, M.; Güemes-Vera, N.; Chanona-Pérez, J.J.; Perea-Flores, M.d.J.; Arzate-Vázquez, I.; Quintero-Lira, A.; Sánchez-Fuentes, C.E. Study of cellular architecture and micromechanical properties of cuajilote fruits (*Parmentiera edulis* D.C.) using different microscopy techniques. *Microsc. Res. Tech.* **2021**, *84*, 12–27. [[CrossRef](#)] [[PubMed](#)]
66. Pavasant, P.; Apiratikul, R.; Sungkhum, V.; Suthiparinyanont, P.; Wattanachira, S.; Marhaba, T.F. Biosorption of Cu²⁺, Cd²⁺, Pb²⁺, and Zn²⁺ using dried marine green macroalga *Caulerpa lentillifera*. *Bioresour. Technol.* **2006**, *97*, 2321–2329. [[CrossRef](#)]
67. Imran, M.; Anwar, K.; Akram, M.; Shah, G.M.; Ahmad, I.; Samad Shah, N.; Khan, Z.U.H.; Rashid, M.I.; Akhtar, M.N.; Ahmad, S.; et al. Biosorption of Pb (II) from contaminated water onto *Moringa oleifera* biomass: Kinetics and equilibrium studies. *Int. J. Phytoremediation* **2019**, *21*, 777–789. [[CrossRef](#)] [[PubMed](#)]
68. Mashentseva, A.A.; Aimanova, N.A.; Parmanbek, N.; Temirgazyev, B.S.; Barsbay, M.; Zdorovets, M.V. *Serratula coronata* L. Mediated Synthesis of ZnO Nanoparticles and Their Application for the Removal of Alizarin Yellow R by Photocatalytic Degradation and Adsorption. *Nanomaterials* **2022**, *12*, 3293. [[CrossRef](#)] [[PubMed](#)]
69. Parmanbek, N.; Sütekin, D.S.; Barsbay, M.; Mashentseva, A.A. Hybrid PET Track-Etched Membranes Grafted by Well-Defined Poly(2-(dimethylamino)ethyl methacrylate) Brushes and Loaded with Silver Nanoparticles for the Removal of As(III). *Polymers* **2022**, *14*, 4026. [[CrossRef](#)] [[PubMed](#)]
70. Khanmohammadi, S.; Musharavati, F.; Tariq, R. A framework of data modeling and artificial intelligence for environmental-friendly energy system: Application of Kalina cycle improved with fuel cell and thermoelectric module. *Process. Saf. Environ. Prot.* **2022**, *164*, 499–516. [[CrossRef](#)]

Disclaimer/Publisher’s Note: The statements, opinions and data contained in all publications are solely those of the individual author(s) and contributor(s) and not of MDPI and/or the editor(s). MDPI and/or the editor(s) disclaim responsibility for any injury to people or property resulting from any ideas, methods, instructions or products referred to in the content.